REPORT OF FULL-SCALE LABORATORY ROTOR BLADE TESTING ACCORDING TO IEC/TS 62600-3

Test Contractor	FastBlade
Test Location:	Building 29 Watt Rd, Rosyth, Dunfermline KY11 2XH
Test Date:	01/01/22-10/08/22
Tested By:	Dr.Fergus Cuthill, Peter Williams, Scott Sinclair, Ondrej Halouzka
Authors:	Fergus Cuthill, Peter Williams
Checked By:	Dr Sergio Antonio Lopez Dubon
Approved By:	Dr Eddie McCarthy, Prof. Dilum Fernando,
Report Date:	29/08/2022

Table of contents

List of Figures

List of Tables

Nomenclature

Acronyms

CAD	Computer Aided Design
cDAQ	Compact Data Acquisition Chassis
CoG	Center of Gravity
cRIO	Compact Real-time Input/ Output Control Chassis
DIC	Digital Image Correlation
EMEC	European Marine Energy Centre
FFT	Fast Fourier Transform
ITH	ITH Bolting Technology Company
MD	Multi-Directional Laminate
MDF	Medium Density Fibreboard
PCD	Pitch Circle Diameter
PID	Proportional Integral and Differential control system
SME	Sustainable Marine Energy
Str_Ros	Strain Gauge Rosette
t/c	Thickness to Chord Ratio
TSN	Time Sensitive Network
UD	Unidirectional Laminate

List of Symbols

δ	Damping vibration time period
ρ	Density (kg/m^3)
ζ	Damping Ratio
F_D	Drag Force (N)
F_L	Lift Force (N)
n	Cycle count

R	Load Ratio (Minimum Load/Maximum Load)
x_0	Amplitude of the first peak
x_n	amplitude of the n^{th} peak

1 Introduction

1.1 Scope

The Scope of this report is to give a detailed account of the tests carried out by the University of Edinburgh on the Deepgen III tidal turbine blade, free issued by the European Marine Energy Centre: EMEC. One static and one fatigue load case, defined by the project partners at Oxford University, were carried out. Deflection, strain, position, applied load, acceleration and temperature were logged throughout the test.

1.2 Test Objectives

1. Define the static and fatigue testing load cases.
2. Define the instrumentation requirements to maximise useful data capture.
3. Carry out static tests to assess blade material properties and validate numerical models.
4. Carry out accelerated full lifetime fatigue test to identify failure mechanisms.
5. Measure natural frequency before and after testing to identify any loss of stiffness as a result of the testing.

2 Blade Identification and Description

2.1 Summary of Blade Dimensions

The blade is part of the DeepGen tidal project and was designed by Tidal Generation Limited (TGL) and manufactured by Aviation Enterprises Limited. The final blade design report is from 2008 and the company responsible for the blade design no longer exists. The rights were bought by another company (Airborne) but some of the design documents were lost and were not provided to FastBlade prior to testing. A detailed description of the geometry of the 5.25m long blade as well as the layup were provided and are given in the following section, no information was available on the blade mass and centre of gravity location. Also, the static and fatigue design loads were provided but no information was given on predicted blade deflections and stresses when exposed to the design loads. The blade was taken from the decommissioned 500kW tidal stream turbine which was previously installed at EMEC's grid connected test site at the Fall of Warness.

Figure 2.1: TGL Blade [1]

2.2 Blade Specifications

2.2.1 Blade Design

A technical drawing of the Tidal Generation Limited blade, looking from the top is shown in Figure 2.2, which was taken from the TG-RE-040-0091, Deepgen Blade Design Report [2]. The blade transitions from a circular root containing a spheroidal graphite cast iron root fitting, containing bolt holes, allowing for a simple connection to the pitch bearing. In the drawing, the two centre lines represent the locations of the shear webs. The spar cap is located between the two shear webs, both on the suction and pressure side of the blade. The entire blade is covered with an 8mm thick glass fibre skin manufactured using $\pm 45^{\circ}$ unidirectional glass fibre prepreg. The dashed lines in Figure 2.2 which are perpendicular to the blade span represent the locations of pairs of 3 mm thick

glass fibre ribs, used to stiffen the blade. They allow for the transfer of pressure from the blade skins to the spar caps and are manufactured using ±45° glass fibre unidirectional prepreg. The spar cap is manufactured using 80% unidirectional carbon fibre epoxy prepreg with the remaining 20% containing 90° fibres to improve the transverse strength and stiffness of the spar region. The shear webs are designed to resist the flapwise shear loads and torsional bending of the blade and are manufactured using ±45° carbon fibre epoxy prepreg. Finally, a rear glass fibre epoxy spar connects the suction side and pressure side 100mm away from the trailing edge to relieve the trailing edge joint from peel stresses.

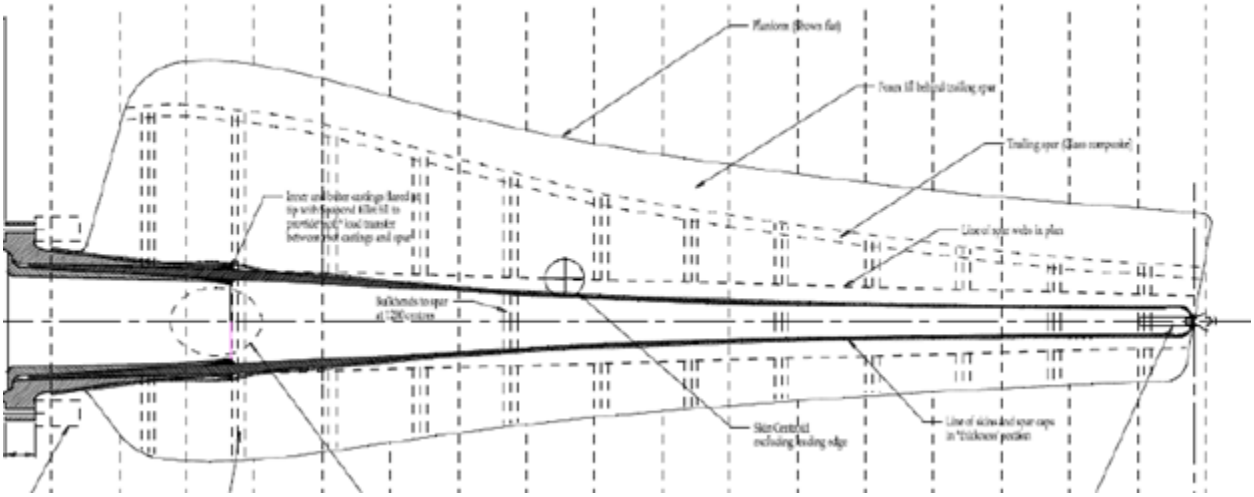

Figure 2.2: Technical Drawing of the Test Blade Looking from the Top View [2]

A view of the cross-section at 3.2m from the blade root, is shown in Figure 2.3, where the main blade regions are identified.

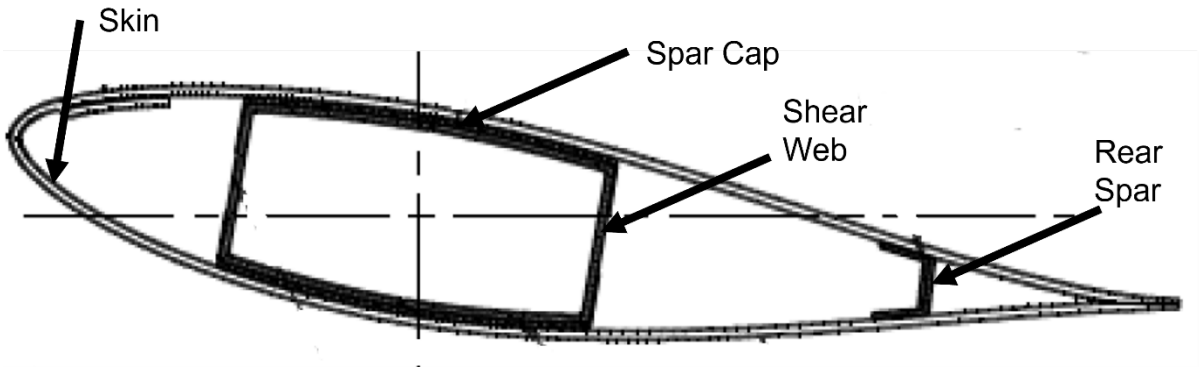

Figure 2.3: Cross-Section at 3.2m from the Blade Root showing the Skin, Spar Cap, Shear Webs and Rear Spar [2]

A detailed distribution of the chord length, pitch angle, aerofoil thickness and thickness to chord ratio (t/c) is given in table 2.1 . Note that the distance along the blade span starts at 1m and ends at 6.25m as the root hub of the DeepGen tidal turbine had a diameter of 2m. At the root, the thickness to chord ratio is 100% as it is a circular section with a diameter of 0.710m. The cross section transitions to an aerofoil with a thickness to chord ratio of around 18%, as shown in Figure 2.4, towards the mid-span of the blade.

Section ID	r (m)	β (deg)	Chord c (m)	Thickness (m) from AEL	t/c ratio
0	1.000	31.9	0.71	0.71	100.00%
1	1.263	27.5	1.23	0.651	52.90%
2	1.525	23.9	1.75	0.592	33.80%
3	1.788	21	1.75	0.532	30.40%
4	2.05	18.6	1.75	0.473	27.00%
5	2.313	16.5	1.69	0.436	25.80%
6	2.575	14.8	1.571	0.399	25.40%
7	2.838	13.4	1.463	0.364	24.90%
8	3.1	12.1	1.367	0.328	24.00%
9	3.363	11.1	1.281	0.294	23.00%
10	3.625	10.1	1.204	0.254	21.10%
11	3.888	9.3	1.134	0.218	19.20%
12	4.15	8.6	1.072	0.187	17.40%
13	4.413	7.9	1.016	0.179	17.60%
14	4.675	7.3	0.965	0.172	17.80%
15	4.938	6.8	0.918	0.164	17.90%
16	5.2	6.3	0.876	0.156	17.80%
17	5.463	5.9	0.837	0.147	17.60%
18	5.725	5.5	0.801	0.139	17.30%
19	5.988	5.2	0.769	0.135	17.60%
20	6.25	4.8	0.738	0.136	18.40%

Table 2.1: DeepGen Blade Cross-Sectional Geometry

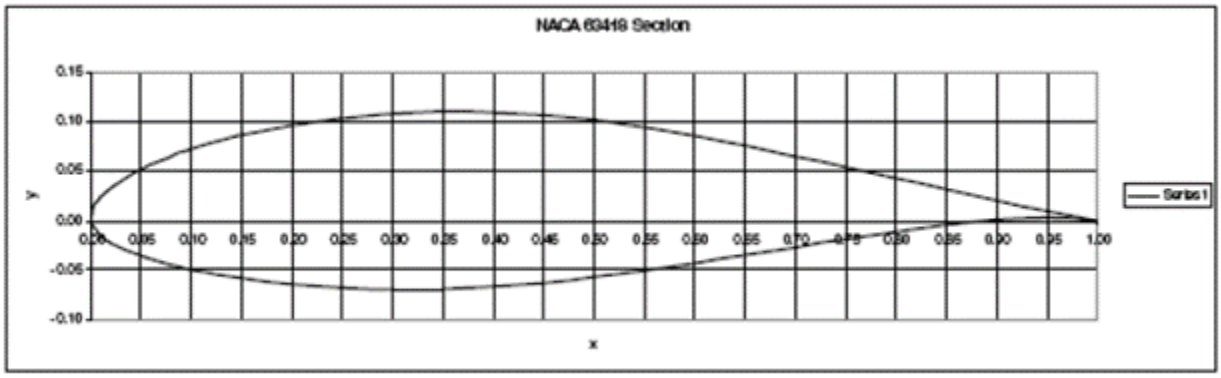

Figure 2.4: Deepgen Aerofoil with 18% Thickness to Chord Ratio [2]

2.2.2 Blade Clamping and Connection to Frame

As mentioned in the previous section, the root of the blade contains a two-part graphite cast iron root fitting. As shown in Figure 2.5, The outer casing is wrapped around the spar cap and shear web and is 1m long. The inner part is placed on the inside of the spar cap and web regions and is 987mm long. The two sections are then attached to each other using 38 M20 evenly spaced bolts. The bolt holes are distributed along a circle with a pitch circle diameter of 560mm from the centre of the root inserts. The outer iron insert is covered by the glass fibre skin and contains a flange

with 30 evenly spaced 48mm diameter holes with a pitch circle diameter of 812mm. These outer holes are used to connect the blade to the pitch bearing using 30 M30 bolts.

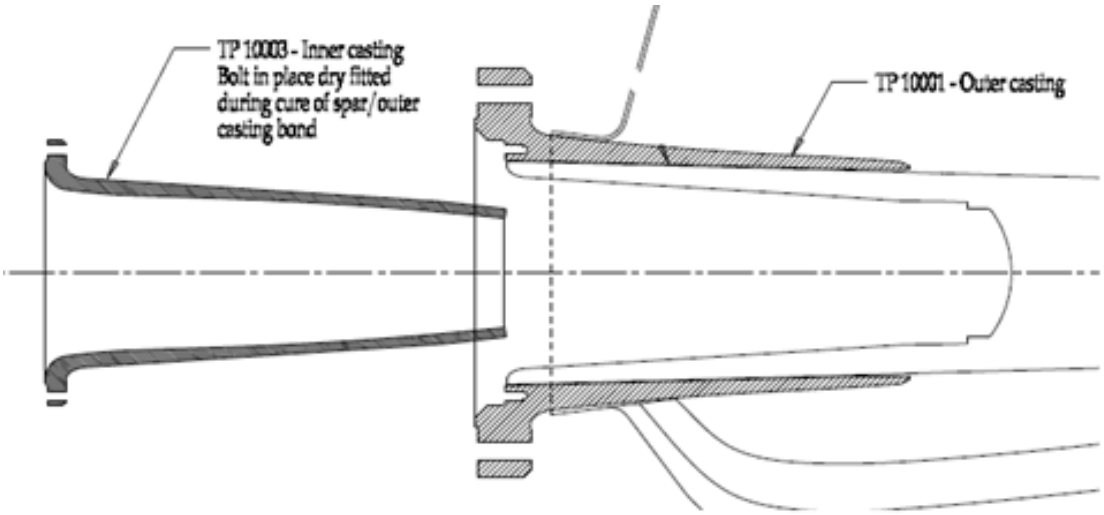

Figure 2.5: Technical Drawing of Cast Iron Root Insert

The introduction of the cast iron inserts leads to a circular bulge visible on the blade near the end of the insert location. This was not predicted in the design process and means that the manufactured blade deviates from the blade design. The heavily distortion in the blade geometry near the end of the insert may lead to local stress concentrations and weakening of the blade. This section of the blade will be investigated with particular attention during testing with the placement of strain gauges in this area.

2.3 Blade Lifting Procedure

Two separate lifting procedures have been proposed for lifting the blade using either one or two gantry cranes. For the single crane life, a stainless-steel threaded insert is included within the blade as shown on the right side of Figure 2.6 allowing for the insert of a lifting eye. A sling is attached around the blade root and connected to the gantry crane via a hook. On the right side, a sling connects the hook to a chain hoist which is attached to the lifting eye at the blade tip through another sling. Introducing a chain hoist between the two slings allows for an adjustment of the length between the hook and the right side of the blade to even tension between the two sides and ensure the blade remains horizontal during the lifting operation. The hook is placed above the centre of gravity of the blade. The slings and chain hoist are rated for a working weight of up to 5 tonnes, which is significantly more than the estimated 1.5 tonne weight of the blade. The gantry cranes are rated for a 10-tonne load.

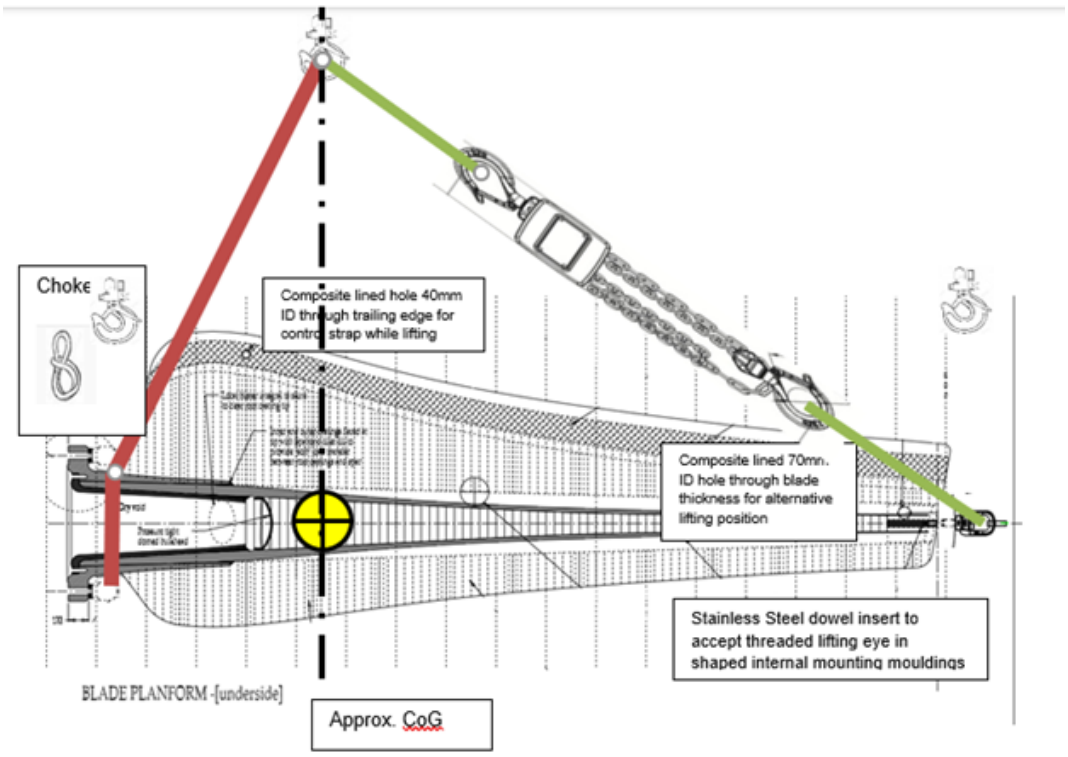

Figure 2.6: Blade Lifting Plan using One Gantry Crane

The lifting procedure using the two gantry cranes of the FastBlade test facility is shown in Figure 2.7. A sling is wrapped around the root of the blade and connected to a first gantry crane via a sling. A similar process is carried out at the blade tip with the sling attached to the lifting eye. This allows finer control of the position of the tip and root of the blade relative to the reaction frame, simplifying the installation procedure.

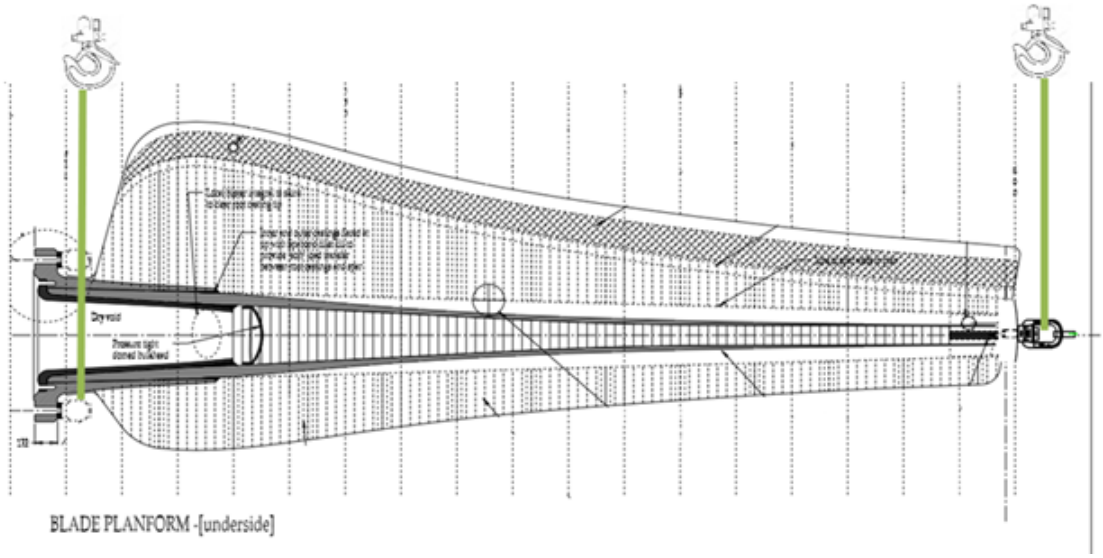

Figure 2.7: Blade Lifting Plan using Two Gantry Cranes

3 Test Equipment

3.1 Test Frame

The reaction frame is used to support all test specimens and load application equipment at Fastblade. It consists of a reaction plane, support wall, T-Slot bed plates and adapter plate, all mounted on bridge bearings. The reaction frame is located in a pit in the floor (2.5m deep) with the top surface of the reaction plane level with the floor of the building. The general layout can be seen in Figure 3.1.

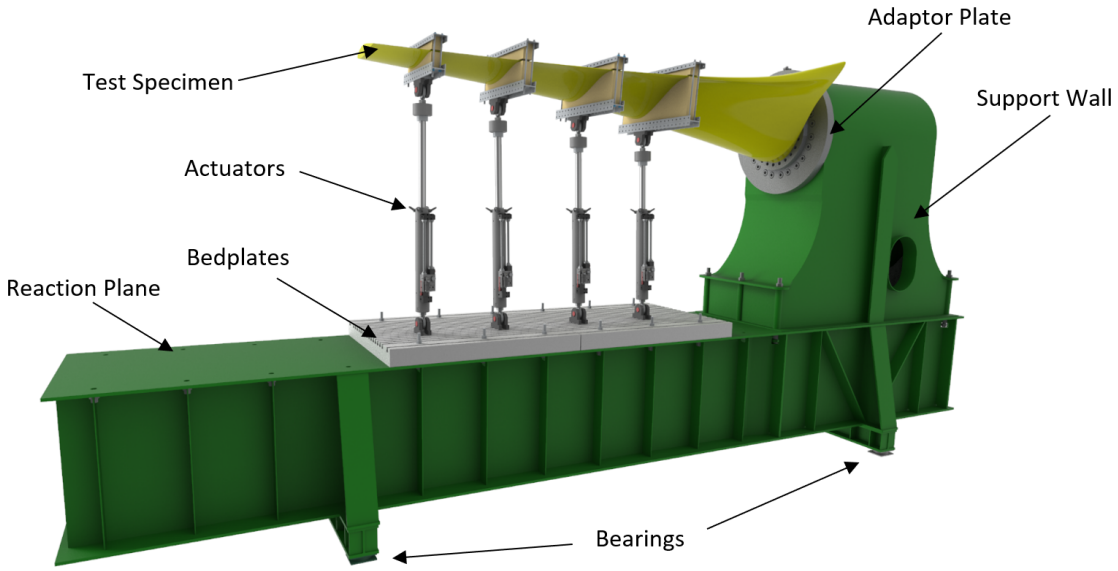

Figure 3.1: Reaction frame general arrangement

There are 3 t-slot bed plates which can be located along the reaction plane as required for mounting either test specimens, support frames or actuators. The general arrangement of the reaction frame along with key dimensions can be seen in Figure 3.3 and 3.2

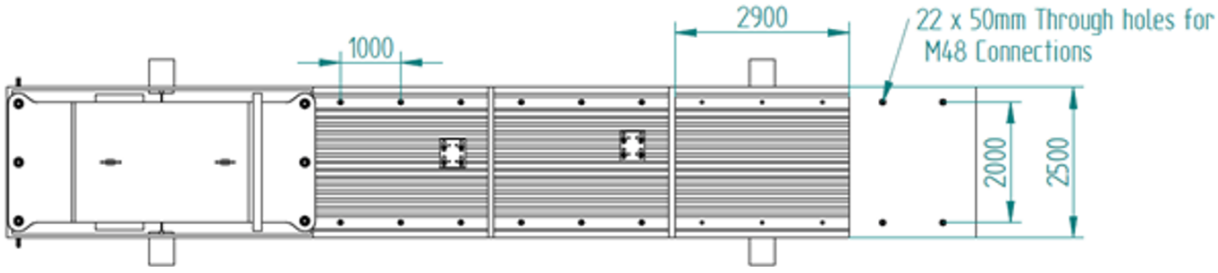

Figure 3.2: Reaction Frame Size - Top view

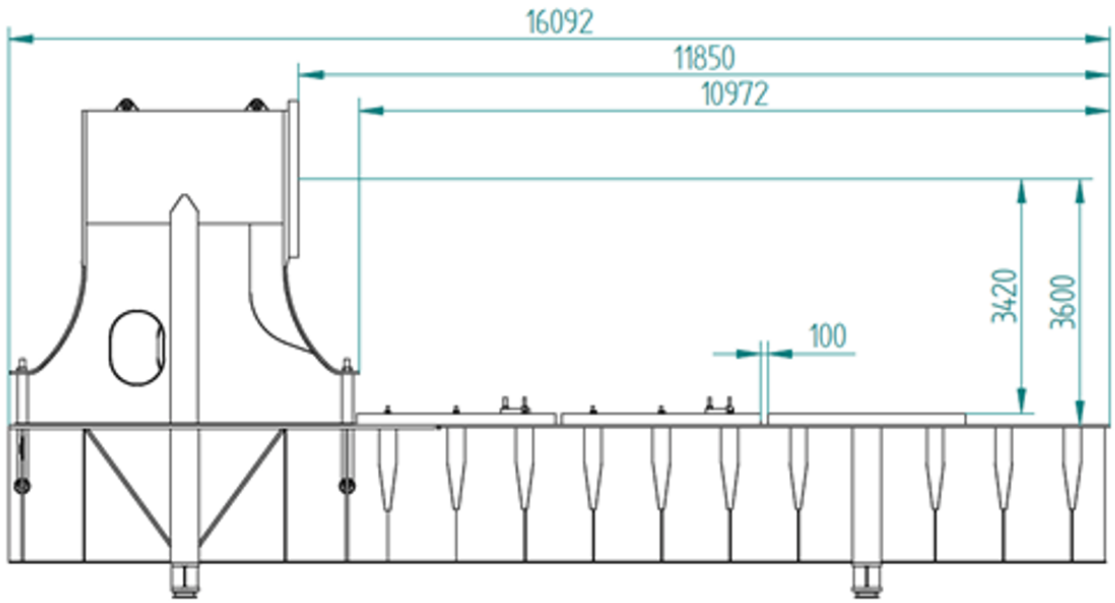

Figure 3.3: Reaction Frame Size - Side view

3.1.1 Strong wall

The strong wall has been designed for mounting tidal blades, however the bolt patterns on the adapter plate can be used for the connection of any specimen type as required. The centre of the adapter plate is located 3.6m above the reaction plane.

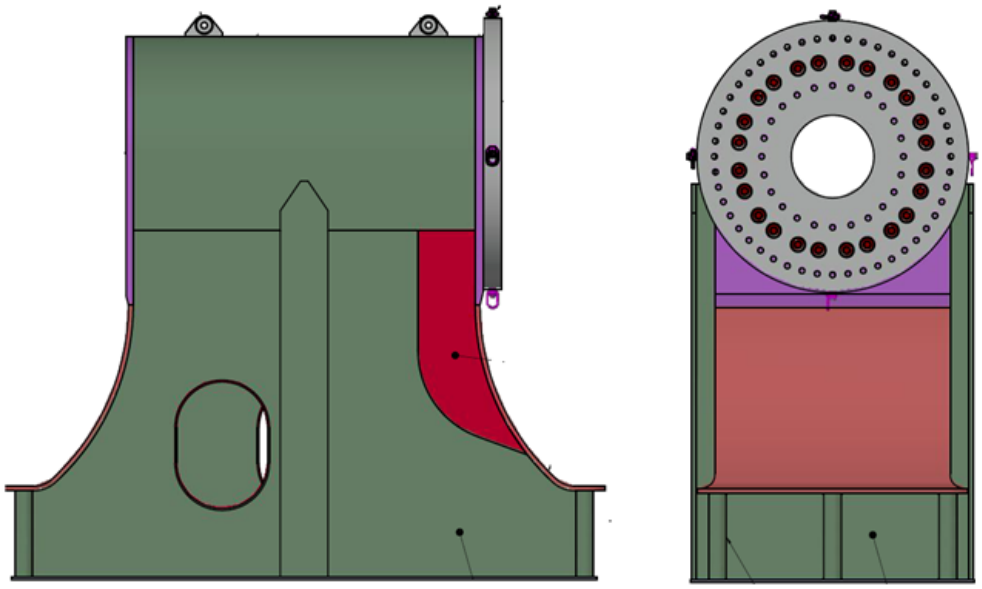

Figure 3.4: Strong wall, adapter mounted.

The adapter plate features 2 different bolt PCD's which may be used for connection to the strong wall. The outer PCD being 48x M48 Tapped holes at 2000mm PCD and the inner being 24x M48 Tapped holes at 1200 PCD.

3.1.2 Strong wall Load Capacity

The strong wall fatigue capacity given below assumes that the load is applied in line with the centre of the reaction frame.

Fatigue Load Capacity	Moment (MNm)	Shear (MN)
FATIGUE (Up to 400 million cycles pushing)	4.7	0.94
FATIGUE (Up to 400 million cycles Pulling)	4.7	0.94
STATIC (Assuming quasi static loading Pulling)	11.955	2.391
STATIC (Assuming quasi static loading Pushing)	10.74	2.148

Table 3.1: Strong Wall Load Capacities

All loadings shown in Table 3.1 assume the individual load limits for bedplates given below are also followed. For any alternative loadings (off axis, torsion) or when operating near these limits individual studies will be required to assess the exact load case.

3.1.3 Frame Flexural Stiffness

In order to quantify the stiffness of the reaction frame a laser was used. The laser was mounted to the strong wall and pointed out to the far wall of the test hall. After applying a 200 kN load to the blade, the angle change of the strong wall was calculated to be 0.00286°.

At this load, the tip deflection of the blade was 82mm. The angle change of the strong wall contributed to 0.26mm of this deflection (0.32%). This is below the 1% threshold as stated in the PD IEC TS 62600-3:2020 A.9.4[3], so can therefore be ignored for the rest of this report.

3.1.4 Blade Connection to Frame

The blade will be attached to the interface plate by connecting 30 M48 bolts between the interface plate and the flange of the cast iron root inserts. At first each of the 30 bolts will be hand tightened. A tensioner is then used to apply a tension of 783 kN to the two red bolts shown on the right side of Figure 14. This corresponds to a tensioner tool pressure of 144.8 MPa. Pressure is supplied to the tensioner by using an ITH pump. Once the two red bolts are tightened, the two blue bolts are tightened next followed by the green and yellow bolt pairs. Then, this sequence of bolt tightening is repeated by moving one bolt clockwise from the red bolt positions. This process is repeated until all bolts are tightened to the correct tension.

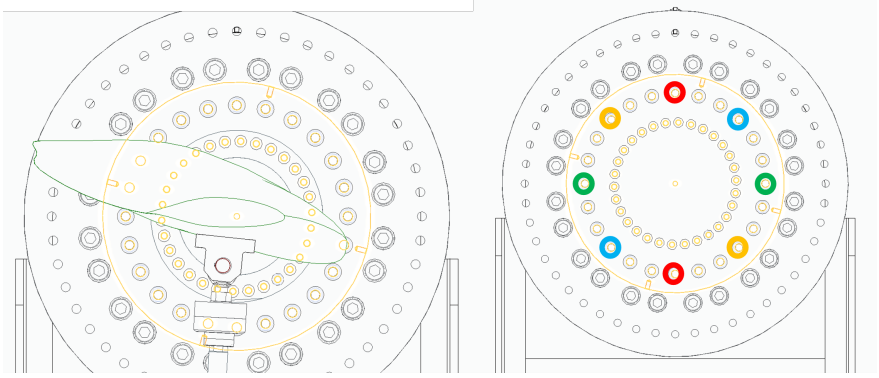

Figure 3.5: Blade Connection to the Interface Plate with Colours Representing the Bolt Tightening Sequence

3.2 Loading Actuators and Hydraulic System

3.2.1 Digital Displacement Pumps

The hydraulic pumps at FastBlade are Digital Displacement pumps supplied by Danfoss (formerly Artemis Intelligent Power). The pumps are unique in their ability to reverse the flow of hydraulic fluid into the hydraulic actuators and recover the energy already put into a test specimen by deforming it. This system allows FastBlade to operate with up to 80% less energy used than similar sized hydraulic systems. The pumps also provide all the control of the actuators, meaning that we can avoid the cost of expensive servo hydraulics and operate with relatively simple actuators. The pumps are located in a pit, alongside the reaction frame. The pit acts as a bund for containing any spills as well as a safety barrier to stop any unauthorised personnel access the pumps. An image of the pumps can be seen in Figure 3.6.

Figure 3.6: Digital Displacement hydraulic pumps during installation in FASTBLADE

3.2.2 Pressure and Flow Capacity

Each pump has a maximum flowrate of 220 LPM, with 4 pumps feeding into a combined high pressure distribution system for a total of 880 LPM. The pumps may be run independently or combined together as required. The pumps have a maximum operating pressure of 420 bar. However, due to the limitations of other components in the system, the maximum we are currently able to operate at is 280 bar.

3.2.3 System Protections

High pressure hydraulic dump valves

There are 8 high pressure dump valves in the system. 4 located at the pumps and another 4 located at the common manifolds at the side of the reaction frame. All 8 valves are triggered by the e-stop system allowing a complete removal of pressure from the high pressure supply lines as soon as

possible and with enough flow capacity to maintain close to zero pressure even if the pumps were still running at their maximum output.

Fixed pressure Relief Valves

There are 4 pressure relief valves at a fixed rating of 420 bar for the protection of the pumps. There are 4 pressure relief valves at a fixed rating of 280 bar for the protection of all other components of the hydraulic system.

Variable pressure relief valves

There are 4 variable pressure relief valves in the system which can be adjusted based on the actuators being used and the desired loads being applied to ensure that the target load is never overshot.

Pump control system limits

Each individual pump can have limits set for both flowrate and pressure for system and specimen protection these sensors operate independently of the main FastBlade control system.

Main Control system limits

The main control system can have limits set on any channel including load, strain, pressure, and displacement. The limits can be set to cause either a full e-stop if triggered or a controlled shutdown of the pumps to a safe level.

3.2.4 Actuators

The current actuators in place at FastBlade have the following specifications:

- Stroke – 1000mm
- Bore Diameter – 150mm
- Rod Diameter – 100mm
- Maximum static push force – 495kN
- Maximum static pull force – 275kN
- Maximum fatigue push force 220kN
- Maximum Operating Pressure – 280bar
- Closed length 2520mm
- Open Length 3520mm
- 500kN integrated tension / compression loadcell

Figure 3.7: Hydraulic Actuator Closed (Total face -face length of 2520mm)

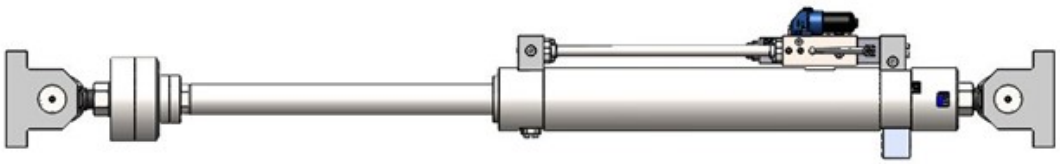

Figure 3.8: Hydraulic Actuator Open (Total face -face length of 3520mm)

3.3 Sensors and Measuring Devices

3.3.1 List of Sensors

Instrument	Manufacturer	Model	Measurement Range	Accuracy/ Non-linearity	Quantity available
Load cell (4-20mA)	Applied Measurements	DSCCFB	±500kN	±0.05% Rated Capacity	4
Load cell (Bridge)	Applied Measurements	DBBSM-2500kg-010-000	±25kN	±0.001% FS	1
Accelerometer (4-20mA)	Omni Instruments	AKF398-10	±10 G	<3% FS	4
Accelerometer (±5V)	TE Connectivity	4030	±6 G	<3% FS	10
Linear Position (4-20mA) (Internal actuator measurements)	MTS	EE Temposonics	0-1000mm	±0.02% FS	4
Strain Gauge Linear	Techni Measure	FRA-3-350-11 (350Ω)	Strain Limit 5%		44 x 350 Ω channels available
Strain Gauge Rosette	Techni Measure	BFLA-5-8 (120Ω)	Strain Limit 3%, composite compensated		16 x 120 Ω channels available
Thermocouple	RS Components	K Type	-200°C to 1260°C		32 Channels
Linear String Potentiometer	Micro-Epsilon	WDS-2000-P96-SR-I	2000mm	±0.1%	2

Table 3.2: List of sensors used at FastBlade

3.3.2 Sensor Locations

The sensor positions on the blade surface are described using a coordinate system, which references lines projected onto the blade surface. The longitudinal lines run between the centre of the root connection to the centre of the lifting eye connection at the blade tip. A description of the longitudinal lines can be found in Table 3.3.

Longitudinal Line Number	Description of Line
1	Projected in line with Xb Axis on blade
2	Projected in line with Yb Axis on blade
3	Manually selected to follow leading edge
4	Bottom side of blade, projected in line with Xb Axis on blade
5	Manually selected to follow top side of trailing edge within 5cm of the edge

Table 3.3: Longitudinal projection definitions (axis defined in figure 4.3)

The crosswise coordinates on the blade are defined as projected lines wrapping around the blade at set distances away from and parallel to the root connection. Crosswise line 1 is located 900mm from the root, all other lines after that are equally spaced at 800mm intervals.

The sensor coordinates are defined using the crosswise line they are on first, followed by the longitudinal line they are on followed by a direction (where appropriate) relative to the longitudinal line they are on. e.g. a strain gauge located at 4-1-P45 would be 3300mm from the root, on the top of the blade, pointing clockwise, 45° from the line following the centre of the blade.

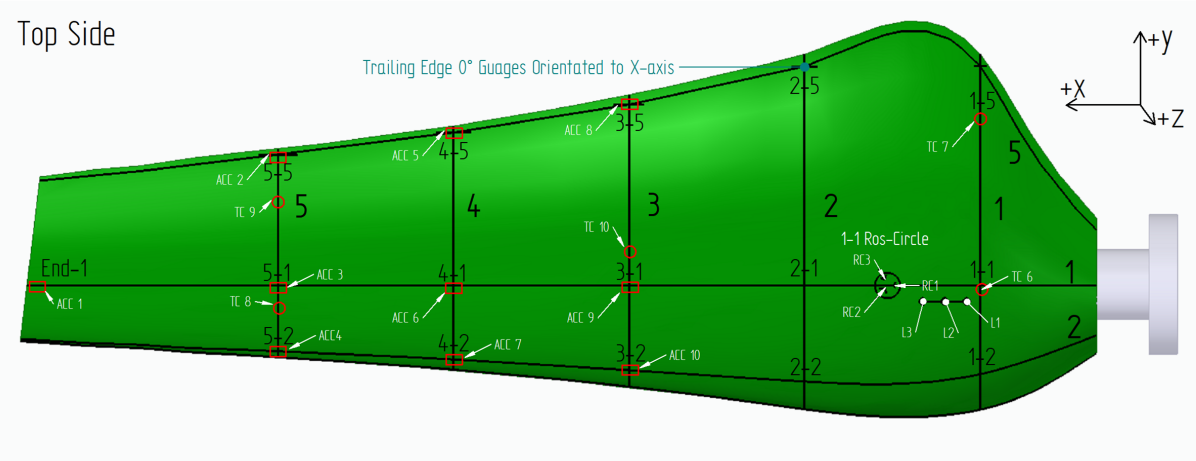

Figure 3.9: Sensor Locations on the top side of the blade

Sensor Location Key			
Coordinates	Strain Guages	Accelerometers	Thermocouples
1-1	Str_Ros_120_1_1_N45 Str_Ros_120_1_1_P45 Str_Ros_120_1_1_0	-	-
2-1	Str_Ros_120_2_1_N45 Str_Ros_120_2_1_P45 Str_Ros_120_2_1_0	-	-
3-1	Str_Ros_120_3_1_N45 Str_Ros_120_3_1_P45 Str_Ros_120_3_1_0	ACC 9	TC 10
4-1	Str_Ros_120_4_1_N45 Str_Ros_120_4_1_P45 Str_Ros_120_4_1_0	ACC 6	-
5-1	Str_Ros_120_5_1_N45 Str_Ros_120_5_1_P45 Str_Ros_120_5_1_0	ACC 3	-
End-1	Linear position draw wire sensor on blade tip	ACC 1	-

Table 3.4: Sensor Position Table 1

Sensor Location Key			
Coordinates	Strain Guages	Accelerometers	Thermocouples
1-2	Str_Ros_350_1_2_N45 Str_Ros_350_1_2_P45 Str_Ros_350_1_2_0	-	TC 6 TC 4
2-2	Str_Ros_350_2_2_N45 Str_Ros_350_2_2_P45 Str_Ros_350_2_2_0	-	-
3-2	Str_Ros_350_3_2_N45 Str_Ros_350_3_2_P45 Str_Ros_350_3_2_0	ACC 10	-
4-2	Str_Ros_350_4_2_N45 Str_Ros_350_4_2_P45 Str_Ros_350_4_2_0	ACC 7	-
5-2	Str_Ros_350_5_2_N45 Str_Ros_350_5_2_P45 Str_Ros_350_5_2_0	ACC4	TC 8 TC 1

Table 3.5: Sensor Position Table 2

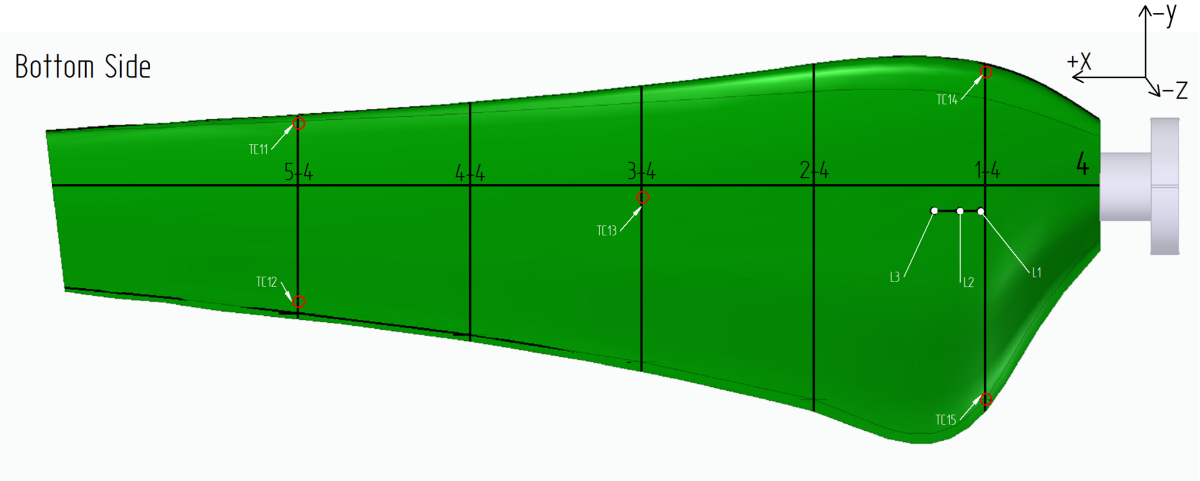

Figure 3.10: Sensor Locations on the bottom side of the blade

Sensor Location Key			
Coordinates	Strain Guages	Accelerometers	Thermocouples
1-3	Str_Ros_350_1_3_N45 Str_Ros_350_1_3_P45 Str_Ros_350_1_3_0	-	-
2-3	Str_Ros_350_2_3_N45 Str_Ros_350_2_3_P45 Str_Ros_350_2_3_0	-	-
3-3	Str_Ros_350_3_3_N45 Str_Ros_350_3_3_P45 Str_Ros_350_3_3_0	-	-
4-3	Str_Ros_350_4_3_N45 Str_Ros_350_4_3_P45 Str_Ros_350_4_3_0	-	-
5-3	Str_Ros_350_5_3_N45 Str_Ros_350_5_3_P45 Str_Ros_350_5_3_0	-	-

Table 3.6: Sensor Position Table 3

Sensor Location Key			
Coordinates	Strain Guages	Accelerometers	Thermocouples
1-4	Str_Ros_120_1_4_N45 Str_Ros_120_1_4_P45 Str_Ros_120_1_4_0	-	-
2-4	Str_Ros_120_2_4_N45 Str_Ros_120_2_4_P45 Str_Ros_120_2_4_0	-	-
3-4	Str_Ros_120_3_4_N45 Str_Ros_120_3_4_P45 Str_Ros_120_3_4_0	Linear position draw wire sensor on blade centre	TC 3 Linear
4-4	Str_Ros_120_4_4_N45 Str_Ros_120_4_4_P45 Str_Ros_120_4_4_0	-	-
5-4	Str_Ros_120_5_4_N45 Str_Ros_120_5_4_P45 Str_Ros_120_5_4_0	-	-

Table 3.7: Sensor Position Table 4

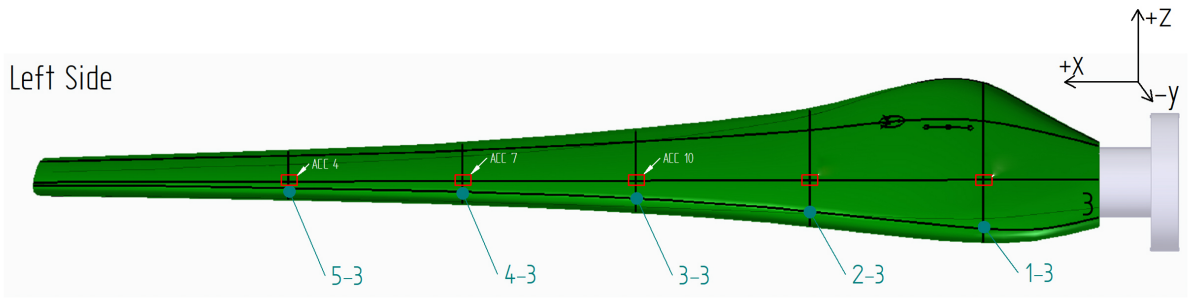

Figure 3.11: Sensor Locations on the leading edge of the blade

Sensor Location Key			
Coordinates	Strain Guages	Accelerometers	Thermocouples
1-5	Str_Ros_350_1_5_N45 Str_Ros_350_1_5_P45 Str_Ros_350_1_5_0	-	TC 7 TC 5
2-5	Str_Ros_350_2_5_N45 Str_Ros_350_2_5_P45 Str_Ros_350_2_5_0	-	-
3-5	Str_Ros_350_3_5_N45 Str_Ros_350_3_5_P45 Str_Ros_350_3_5_0	ACC 8	-
4-5	Str_Ros_350_4_5_N45 Str_Ros_350_4_5_P45 Str_Ros_350_4_5_0	ACC 5	-
5-5	Str_Ros_350_5_5_N45 Str_Ros_350_5_5_P45 Str_Ros_350_5_5_0	ACC 2	TC 9 TC 2

Table 3.8: Sensor Position Table 5

Sensor Location Key			
Coordinates	Strain Guages	Accelerometers	Thermocouples
1-1-Lin	Str_Lin_120_L1_1_1_0 Str_Ros_120_L2_1_1_0 Str_Ros_120_L3_1_1_0	-	-
1-4-Lin	Str_Lin_120_L1_1_4_0 Str_Lin_120_L2_1_4_0 Str_Lin_120_L3_1_4_0	-	-
1-1-Ros Circle	Str_Ros_350_RC1_N45 Str_Ros_350_RC1_P45 Str_Ros_350_RC1_0 Str_Ros_350_RC2_N45 Str_Ros_350_RC2_P45 Str_Ros_350_RC2_0 Str_Ros_350_RC3_N45 Str_Ros_350_RC3_P45 Str_Ros_350_RC3_0	-	-

Table 3.9: Sensor Position Table 6

3.3.3 Digital Image Correlation Equipment (DIC)

Two sets of stereo pair cameras were used to capture different regions of the blade. The first set was positioned approximately 4m away from the blade using 12mm lenses in order to capture the entire surface of the blade between the root connection and the saddle. The speckle pattern was applied using a compressed air spray gun to initially apply a coat of matt white paint. This was followed by using a silicone rubber sheet with laser-cut holes as a stencil to apply the black matt spray,

forming the speckles. The speckles were 6mm in diameter covering approximately 3.5m length of the blade.

The second set of cameras was focused on a much smaller area of the blade, at the transition from the metal hub connection to full composite, approximately 800mm from the root of the (indicated in figure 6.16. This section had an extremely fine speckle pattern with speckles printed onto tattoo paper using a laser printer at a size of 0.1mm diameter. This was then applied to an area of approximately 20cm x 20cm for a high-resolution view of the transition from steel to composite.

The cameras being used were FLIR Blackfly S (BFS-U3-88S6M-C) 8.9MP, logging images at 1 Hz throughout the static test.

3.4 Sensor Calibration

3.4.1 Strain Gauges

After being carefully positioned, glued and wired, the strain gauges were calibrated using the manufacturer settings for the gauge resistance as well as the gain. The strain gauges were zeroed prior to beginning each test to account for the thermal variation day to day of the testing

3.4.2 Accelerometers

The accelerometers were calibrated using calibration data supplied by the manufacturer. The accelerometers were never zeroed during testing. Accelerometer data was validated before testing by rotating the accelerometers through their axis on a flat level surface to confirm the correct measurement of gravity was given.

3.4.3 500kN Load Cell

The load cell was calibrated using calibration data supplied by the manufacturer. It was zeroed prior to commencing testing.

3.4.4 25kN Load Cell (Blade mass measurement)

The load cell was calibrated using calibration data supplied by the manufacturer. It was zeroed prior to commencing testing.

Date	24/07/2019
Rated capacity	24516.625 N
Zero output	0.0041 mV/V
Calibration mode	Tension
Full-scale sensitivity	2.8519 mV/V
Non-linearity	-0.001 +- %/rated capacity
Hysteresis	-0.025 %/rated capacity
Test Excitation	10.000 Vdc
Creep	<0.03%/rated capacity (30 mins)
Electrical connection	10m cable

Table 3.10: Calibration Data

3.4.5 Displacement sensors

The displacement sensors were calibrated using calibration data supplied by the manufacturer. They were zeroed after being connected to the blade but not zeroed between tests.

3.4.6 Thermocouples

The k-type thermocouples were logged using the in-built parameters in the NI Logging system. They were never zeroed during testing.

3.4.7 Digital Image Correlation (DIC)

The DIC system was calibrated at the start of each day of testing. Calibration is carried out using an accurately printed aluminium faced foam board calibration panel, featuring a grid of accurately printed black dots. A series of images are taken of the calibration panel by each of the DIC cameras. The panel is moved within the field of view at different angles and rotations to provide the system with movement in all 3 axes in order to perform a complete calibration. Between 120 and 200 images were taken for each calibration. The system can then calculate the intrinsic parameters (focal length, optical centre, lens distortions etc) and the extrinsic parameters (Relative angles and positions of cameras). The calibration of each of the 2 cameras were then combined to create a calibrated stereo setup.

3.5 Pre-Test Calibration

At the beginning of every test, after the appropriate signals had been zeroed. A "zero reading" was taken, where a 10 second log file was recorded with no motion of any components of the system in order to have a baseline to which we can reference changes throughout the tests. This zero reading was taken before each of the static tests and the fatigue test.

3.6 Data Acquisition System

The data acquisition system uses 4x NI cDAQ 9189 chassis all synchronised together using a time sensitive network (TSN) to provide a reliable distributed logging system. With the chassis are various C-Series modules for logging the different signal types. See table 3.11 for module types and accuracies.

Module	Signal Type	Percent of Reading (Typical gain error)	Percent of Range (Typical offset error)	Measurement Resolution
9203	4-20mA Current	±0.49%	±0.46%	16 Bit
9237	Strain / Bridge	0.20%	0.25%	24 Bit
9205	0-10V Voltage	±1%	N/A	16 Bit
9214	Thermocouple	0.03%	N/A	24 Bit

Table 3.11: NI Modules used at FastBlade

All the data logging is controlled via Flexlogger software from the control room. This software allows for visualisation and logging of all signals during a test. The Flexlogger software does not allow control of the test. Control is carried out on a real time NI controller (NI cRIO 9049) which shares the load signals so that the test control and logging system both have access to the load cell data.

4 Test Setup and Procedures

4.1 Test Sequence

The test sequence followed during this test program is described in Table 4.1. Prior to static testing, the weight of the blade and the location of the centre of gravity were determined. Then, the blade was positioned for the first static test. A natural frequency test was carried out in this position followed by the static test and then another natural frequency test. The same process was repeated for the fatigue test. Finally, the static test was repeated after the fatigue test to ensure the structural integrity of the blade was maintained at the end of the test program. This section gives a description of the individual test procedures mentioned in Table 4.1.

Order	Test Case
1	Mass and COG Determination
2	Setup Load Case 1 in Xb Direction
3	Natural Frequency (3 Repeats)
4	Apply Static Load
5	Natural Frequency (3 Repeats)
6	Apply Fatigue Load
7	Natural Frequency (3 Repeats)
8	Apply Static Load
9	Natural Frequency (3 Repeats)

Table 4.1: Test Sequence

4.2 Weight and Centre of Gravity Measurement

To measure the blade weight and the location of the centre of gravity (CoG) measured as a distance from the blade root, a process similar to the lifting procedure using one gantry crane shown in Figure 2.6 was carried out. However, an additional sling was connected to the gantry crane via a load cell. The chain hoist position was adjusted until the blade was stable and level when being lifted from a single point. A plumb line and a vertical laser level were then used to identify the CoG on the surface of the blade, as well as a measurement of the blade weight.

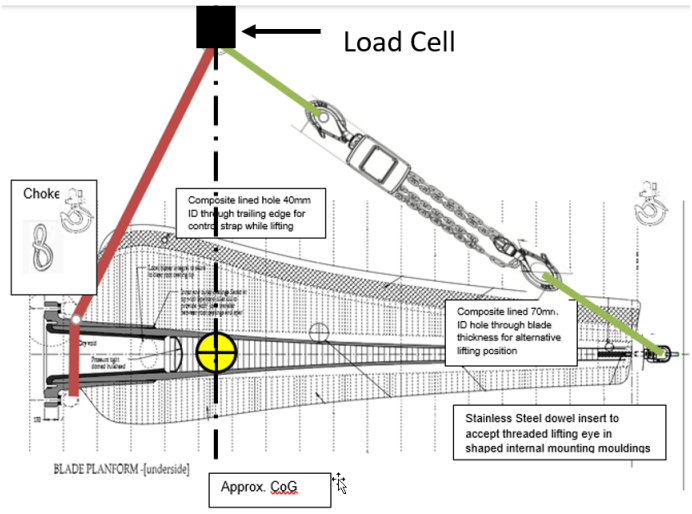

Figure 4.1: Weight and Centre of Gravity Measurement Procedure

4.3 Natural Frequency and Damping Test

With the blade bolted to the reaction frame and the accelerometers installed on the blade, the blade was hit in the flapwise direction with a rubber mallet to excite the blade at its natural frequency. By performing a Fast Fourier transform (FFT) on the time-series accelerometer data, the frequency domain response of the blade were obtained. The peaks in the frequency domain response correspond to the natural frequencies of the blade.

As the natural frequency of a structure is dependent on its stiffness, any damage detrimental to the structure should be observed in the form of a reduction in the measured natural frequency. This is why a natural frequency and damping test is carried out at the beginning of the test program, between the static and fatigue tests, after the fatigue test, and finally at the end of the final static test. It ensures that any reduction in the mechanical properties of the blade can be detected rapidly before moving on to the following test. The damping ratio of the blade can also be measured using the time series accelerometer data captured during the free vibration of the blade as shown in Figure 4.2. Using the height of successive peaks and equations 4.1 and 4.2, the damping ratio can be calculated.

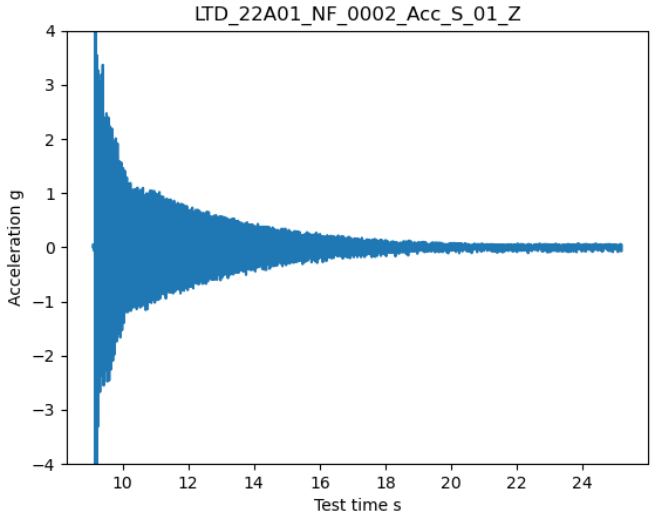

Figure 4.2: Time Series Accelerometer Data following a Blade Perturbation

$$\delta = \frac{1}{n} \cdot \frac{\ln(x_0)}{\ln(x_n)} \tag{4.1}$$

$$\zeta = \frac{1}{\sqrt{1 + \left(\frac{2\pi}{\delta}\right)^2}} \tag{4.2}$$

4.4 Test Setup

4.4.1 Load Direction

The loading direction was based on the documentation available in the Extreme and Fatigue Load Calculations for Deepgen 500kW Tidal Turbine [4] which describes the axis systems for the blade, as shown in Figure 4.3 as well as the magnitude of the expected loading for these directions. By combining the loading in the XB and YB directions an actuator angle of 14.58° anti-clockwise from the XB axis when viewed from the blade tip, was identified as the optimal loading direction, as shown in (a) from Figure 4.4. However, for practical installation reasons, the loading direction was chosen to be along the XB Axis as shown in (b) from Figure 4.4. This allowed the hydraulic actuator to contact the blade in a way that simplified the clamping system for the saddle connection to the blade. As this was also the first test of the FastBlade facility it was decided that a simple, more reliable loading would provide more useful results.

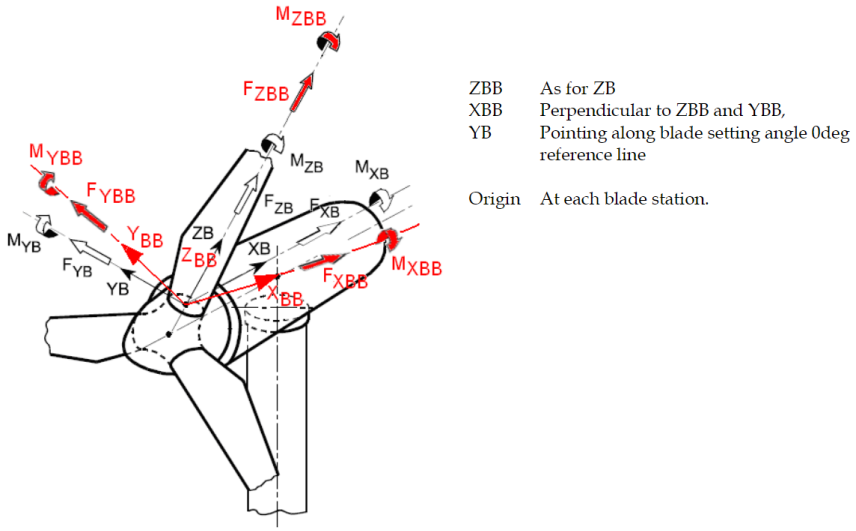

Figure 4.3: Co-ordinate system for blade loads (pitching frame of reference)

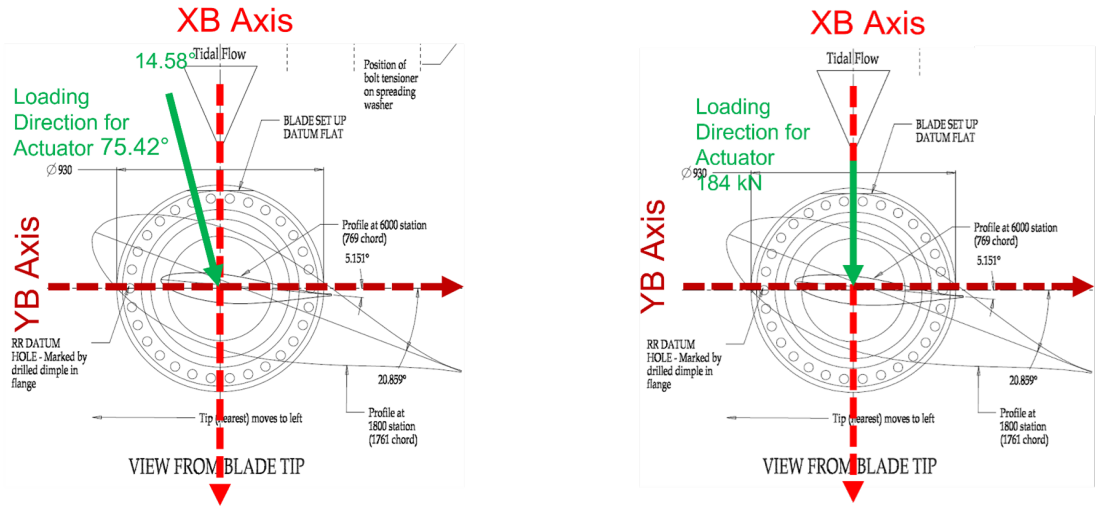

(a) Extreme Design Load for Deepgen Blade

(b) Load Cases Actually Tested

Figure 4.4: Load Cases for Testing

4.4.2 Load Introduction

In order to apply the required loads to the blade, a method of distributing the force from the hydraulic actuator into the structure of the blade was required. Two methods were trialled for this process. Firstly, an articulated pad system, as shown in Figure 4.5. This allowed the load to be distributed over 4 individual pads which would move with the blade during the testing. This system would not introduce any additional bending moments to the specimen which are often seen with clamped systems, however, the lack of constraint also meant the alignment of the pads was extremely difficult and pad slipping was observed. The slippage occurred in the Y direction (defined by axis in Figure 3.10), towards the trailing edge. The movement was slow and continuous throughout the static test. The total distance travelled was over 100mm.

Figure 4.5: Articulated pad, load introduction system

The second load introduction method was a clamped wooden saddle with a steel surrounding frame and a 1.5mm thick silicone sheet at the blade interface. This system can be seen in Figure 4.6. In order to manufacture a fitted saddle like this, a 3D scan of the blade was taken. The scan was then sliced into 25mm segments which could be cut out of MDF boards and attached together to form an accurately fitted system for distributing the load into the surface. This has several advantages over the articulated pad saddle. It does not move during testing, once connected it remains aligned meaning the pads don't have to be re-aligned every time the hydraulic system was shut down and re-started. The rigid clamping can induce additional bending and constraints on the blade. Several studies, [5] [6] have been carried out which suggest that the additional bending on the blade would not be sufficient to affect the failure mode of a full-scale tidal blade, which is still expected to be located near the blade root. Therefore, it was decided that the benefits of the continually connected saddle outweighed the negative side effects.

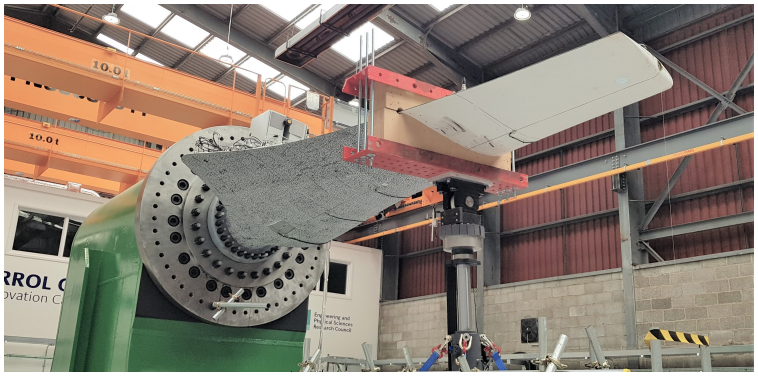

Figure 4.6: MDF fitted load introduction system

4.5 Static Tests

The static load was chosen based on the most extreme load case listed in the load cases document [4] provided about the turbine. The highest load case was a 970.2 kNm root bending moment about the YBB axis. By using a load location script, developed in-house, to identify optimal locations for any number of hydraulic rams to match a given bending moment distribution, an actuator location of 3.5495m from the back face of the blade connection flange, pushing in the XBB direction with a target load of 273.33 kN was identified as the loading location achieving the moment about the YBB axis.

4.6 Fatigue Tests

The fatigue load was chosen based on the data provided about the site where the turbine was deployed. The data was provided as part of the ReDAPT project, Metocean Data set [7] [8]. By analysing the data, Oxford University identified the most common tidal flow speed to be 2.8 m/s. They simulated the loads this flowrate would apply to the blade in every tidal cycle at this flow speed, giving a root bending moment of 652.1 kNm. At the same actuator position as the static test, this gives a target load of 183.7 kN.

One of the practical limitations of regenerative fatigue testing at FastBlade is that it is not possible to drop to 0 kN to fully remove the load during a test cycle. In order to test while always maintaining a positive pressure in the hydraulic system a load ratio of R = 0.1 is used. Testing was carried out using a sine wave with an amplitude of 82.67 kN and an offset of 101.04 kN. This achieved the target load of 183.71 kN and dropping to a minimum load of 18.37 kN. The test frequency chosen was 1 Hz.

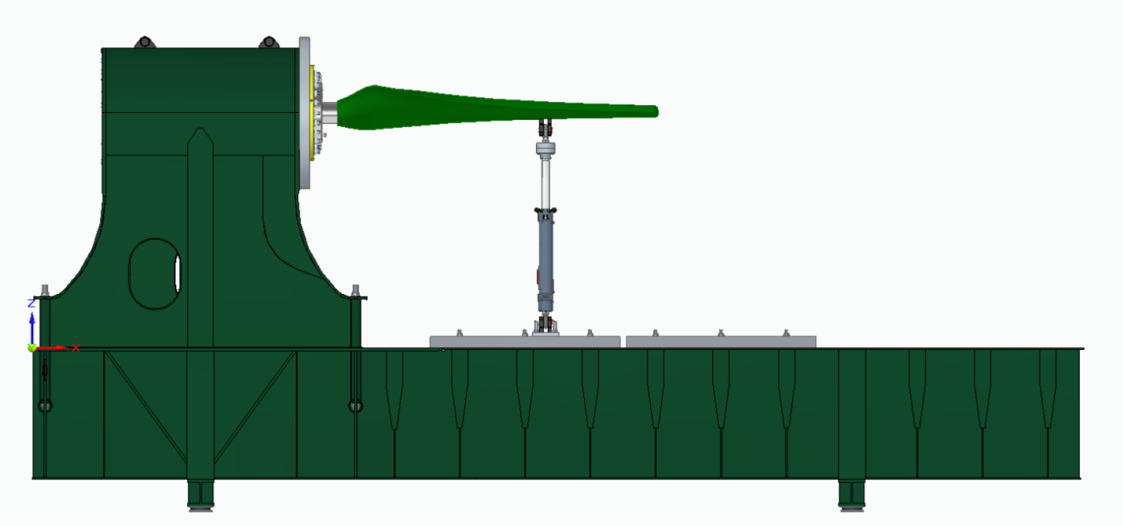

Figure 4.7: Deepgen Blade during Static Testing with the Hydraulic Rams Pushing the Blade in the Vertical Direction

5 Test Uncertainty

5.1 Error on Blade Alignment and Load Introduction Location

The rotational alignment of the blade around its long axis was dependent on the CNC machined adapter plates for the connection to the FastBlade reaction frame. The position of the bolt holes allowed the blade to be aligned to within 3° of its ideal position (Actuator pushing vertically up onto the blade from below). The 3° error was accounted for by angling the actuator to account for the misalignment.

The adapter plate on the reaction frame was machined to be within 0.1° of vertical, providing a vertical reference face for the connection of the blade.

The position of the actuator from the root of the blade was measured using a laser distance meter. The correct location was calculated from the CAD model of the reaction frame and blade, developed during the planning stage of the test.

The saddle was manufactured from a 3D scan of the blade as the manufactured blade did not match the drawings of the blade well enough for the drawings to be used to build a saddle. The 3D scan of the blade also contains errors, however, it was difficult to quantify. To account for this error, a 1.5mm silicone sheet was placed at the interface between the wooden saddle and the blade.

5.2 Error on Sensor Locations

Sensor locations were decided upon within the CAD model of the blade. A laser line was used to project the axis described in CAD onto the curved surface of the blade. The distance from the root to the sensor location was measured using a laser distance meter. Positioning error relative to the CAD model was not possible to accurately determine without more sophisticated equipment. The error is estimated to be +/-5mm.

5.3 Sensor Measurement Errors

Details of the accuracy of each sensor type are listed in table 3.2. However, due to the nature of the test setup, long cable, and a high number of sensors. a larger than specified noise level was present on all sensors. This uncertainty is very difficult to quantify, as levels of noise varied between sensors, and from test to test, depending on what electrical systems were being used and how many sensors were being logged simultaneously.

5.4 Data Acquisition System

Details regarding NI modules used for the data acquisition are listed in table 3.11. The accuracy of each module is indicated in the table. All data is logged using a time-sensitive, synchronised network meaning all measurements are time stamped and synchronised with µs accuracy.

6 Test Results

6.1 Blade Weight

The Loadtide blade was weighed on 14/03/2022 and this report describes the result and process of this weighing. The measuring load cell was zeroed with all rigging equipment present. At the time measurements were taken, previous paint was all sanded off, one side was painted white with DIC speckles, and several gauges were already installed. The blade was weighed with four white Ethernet port hubs on it. Calibration data can be found in table 3.10

Three separate measurements were taken, each over the period of 15 seconds:

Measurement number	**Average [N]**	**Average [kg] ($g = 9.81\ ms^{-2}$)**	**Maximum [N]**	**Minimum [N]**
1	15584.24	1588.61	15586.66	15581.81
2	15584.06	1588.59	15587.03	15580.65
3	15583.90	1588.57	15586.44	15580.85

Table 6.1: Measurement Data

Averaging over the three measurements, obtaining the mass of the blade to be **1588.59kg**, (15584.07 N).

Figure 6.1: Image of the weighing process

6.2 Blade Centre of Gravity

Using the same configuration as seen in Figure 6.1 the CoG is determined. In order to measure the CoG the blade was aligned at 90°to a line vertical from the crane hook. the location of the intersect of the blade and the laser line from the crane hook is the CoG. This was measured from the root of the blade and was found to be located at 900 ± 30 mm from the root.

6.3 Natural Frequency

The natural frequency was measured at the stages of the test described in Table 4.1. However, due to a change in the test process as a result of moving to a clamp-on saddle, the post-fatigue test was carried out with the saddle in place, so is not comparable with the initial tests. A final test at the end was carried out without the saddle attached to the blade to be comparable to the initial tests.

A summary of the natural frequencies measured can be seen in Figures 6.2a & 6.2b, with the actual values shown in Tables 6.2a & 6.2b.

The values shown are only those of the 1st natural frequency, measured in the Z direction (see Figure 3.11) using the accelerometer at the blade tip. Harmonics were detectable up to the 6th harmonic. Natural frequency in the Y direction was measured at approximately 29 Hz. However, for this analysis, all comparisons were made using the first natural frequency in the Z-Direction.

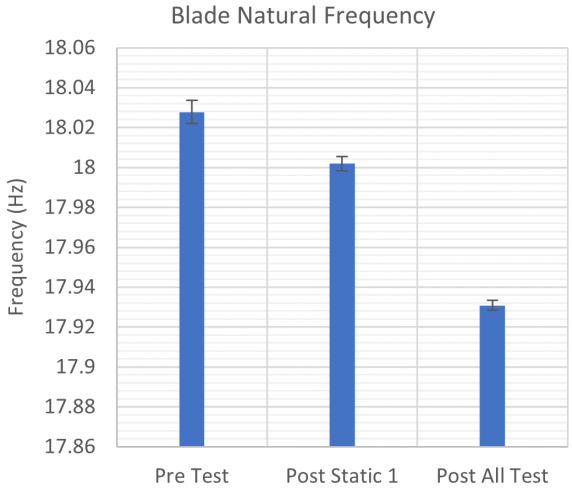

(a) Natural Frequency changes

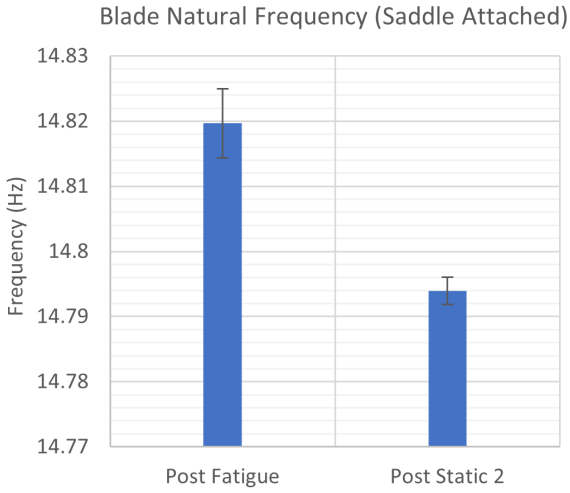

(b) Natural Frequency changes (Saddle Attached)

Figure 6.2: Natural Frequency changes of the blade

	Natural Frequency (Hz)	Standard Deviation
Pre Test	18.0278	0.0057
Post Static 1	18.0019	0.0035
Post All Test	17.9308	0.0026

(a) No Saddle Attached

	Natural Frequency (Hz)	Standard Deviation
Post Fatigue	14.8196	0.0053
Post Static 2	14.7939	0.0021

(b) Saddle Attached

Table 6.2: Data for Natural Frequency of the blade

The main reason for performing the frequency and damping analysis was to identify if any discernible damage occurred in the blade when it was subjected to the load cases. If damage occurred, this would have led to a reduction in the measured natural frequency and a change in the damping ratio. The results from the natural frequency test performed after all testing was complete indicates that the natural frequency has lowered compared to the natural frequency before the first test. The same is true for the damping ratio. This analysis therefore seems to suggest that the blade was damaged during this test program. Although it is not possible to know where/what this damage was without further investigation.

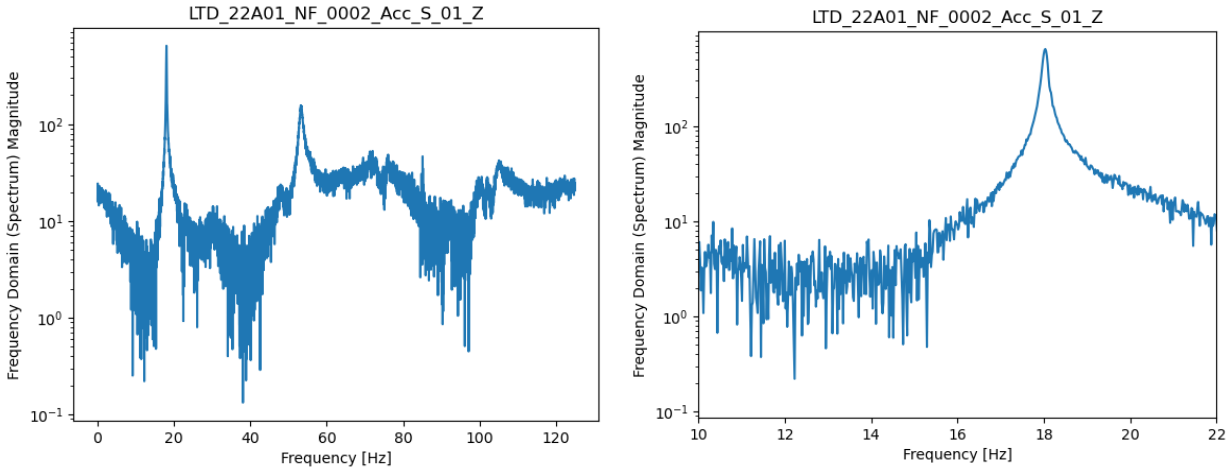

(a) Full Spectrum **(b)** Zoomed

Figure 6.3: Frequency response in the z direction at the tip of the blade - Pre Static

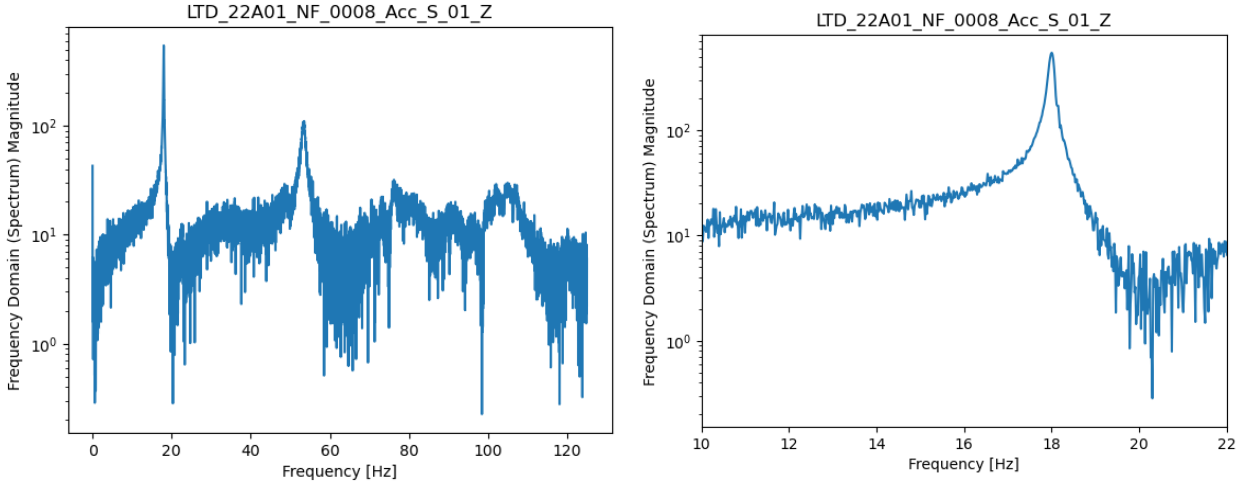

(a) Full Spectrum **(b)** Zoomed

Figure 6.4: Frequency response in the z direction at the tip of the blade - Post Static

Figures 6.3 and 6.4, compare the FFT's of the z direction accelerometer data, from before and after the first static test. The graphs shown are representative of the 3 repeats of each test that were carried out. A zoomed-in area showing the 1st natural frequency is also provided for comparison.

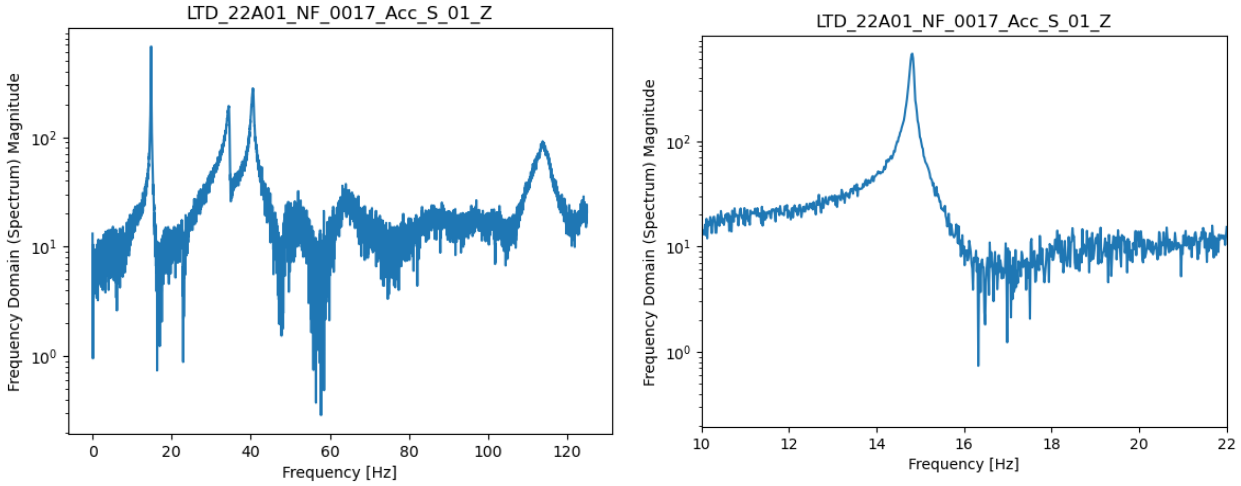

(a) Full Spectrum **(b)** Zoomed

Figure 6.5: Frequency response in the z direction at the tip of the blade - Post Fatigue (with saddle attached)

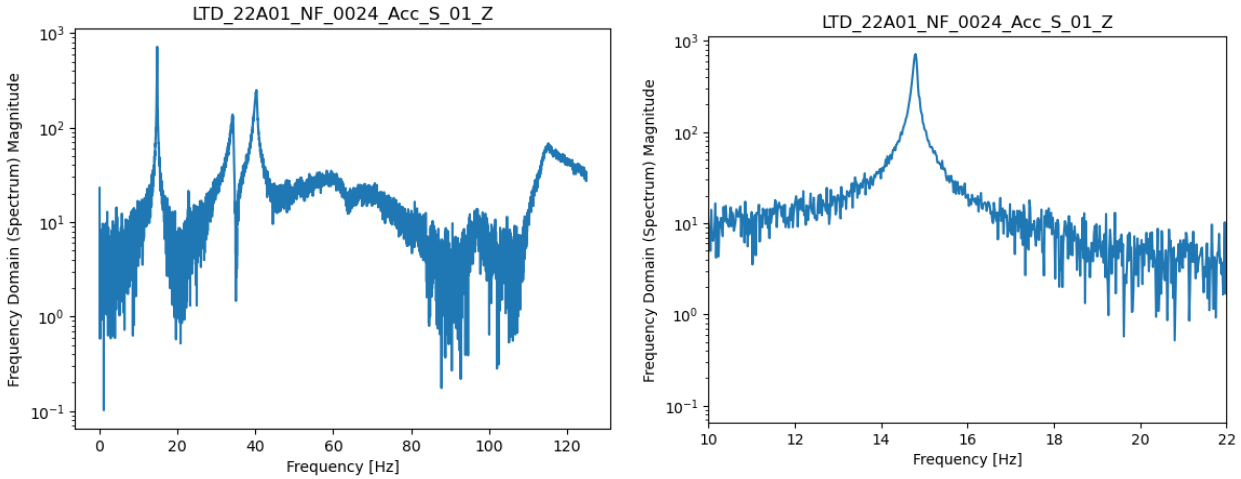

(a) Full Spectrum **(b)** Zoomed

Figure 6.6: Frequency response in the z direction at the tip of the blade - Post Static 2 (with saddle attached)

Figures 6.5 and 6.6, compare the FFT's of the z direction accelerometer data, from before and after the final static test. These tests were carried out with the loading saddle still attached to the blade, meaning they are not directly comparable to the results in Figures 6.3 and 6.4. However, they still indicate a small but measurable reduction in natural frequency from 14.82 Hz to 14.79 Hz. Indicating that further damage continues to be done to the blade during testing. A zoomed-in area showing the 1st natural frequency is also provided for comparison.

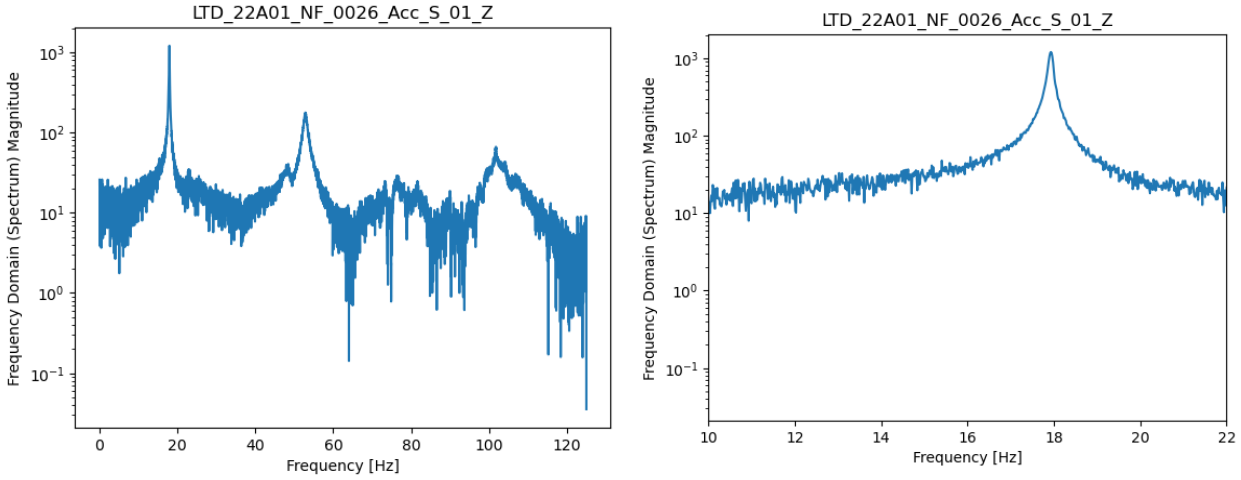

(a) Full Spectrum

(b) Zoomed

Figure 6.7: Frequency response in the z direction at the tip of the blade - Post Static 2 (without saddle attached)

Figure 6.7 shows the final natural frequency test which was carried out. When compared to the results from the initial test in Figure 6.3 it can be seen that the natural frequency has reduced from 18.03 Hz to 17.93 Hz.

6.3.1 Blade Damping

The damping ratio was measured using the logarithmic decrement of the acceleration response of the blade using equations 4.1 and 4.2 from section 4.1

Figure 6.8 shows an example of the damping ratio data as a function of the number of oscillations calculated using the above equations. The damping ratio is not stable but appears to converge after about 120 oscillations. The ratio was calculated for each test using the average after the damping ratio had stabilised (from approximately 120 oscillations on wards).

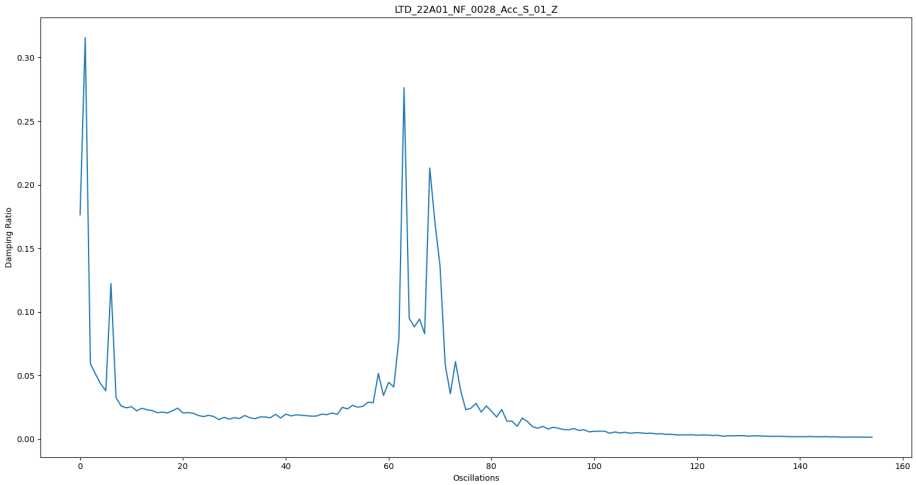

Figure 6.8: Damping ratio vs cycle count for the blade on the reaction frame

Table 6.3 shows the average damping ratio for the 3 initial natural frequency tests along with the 3 final natural frequency tests. The reported error comes from the standard deviation between the damping tests. The lack of stability of the damping coefficient data makes it difficult to draw conclusions but it appears that the damping ratio increases by approximately 23.5% as a result of the testing.

	Damping Ratio	
Test Number	Before Testing	After Testing
1	0.00182	0.00226
2	0.00186	0.00248
3	0.00184	0.00209
Average	0.001841	0.002275
Standard Deviation	1.45E-05	0.000162

Table 6.3: Average damping ratio before and after testing

6.4 Static Test Results

6.4.1 Initial Static Test Run

Static testing was carried out with the following load profile as shown in Figure 6.9. The load was increased from approximately 0 kN (an initial load of exactly 0 kN was not possible due to the setup of the hydraulic system) to 273.33 kN over 120 seconds. The load was then held for 1 hour before returning to near 0 kN over 120 seconds again. This load profile meets the requirements for static testing set out in the IEC 62600-3 standard [3], however, a hold of 6 hours would have been preferable.

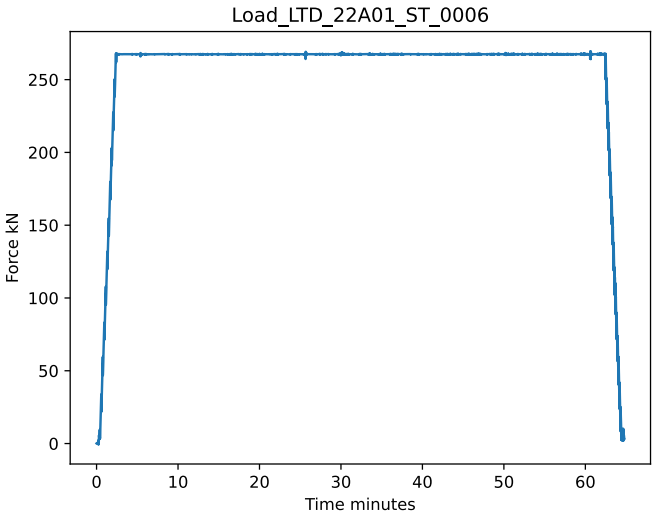

Figure 6.9: Full initial static loading cycle

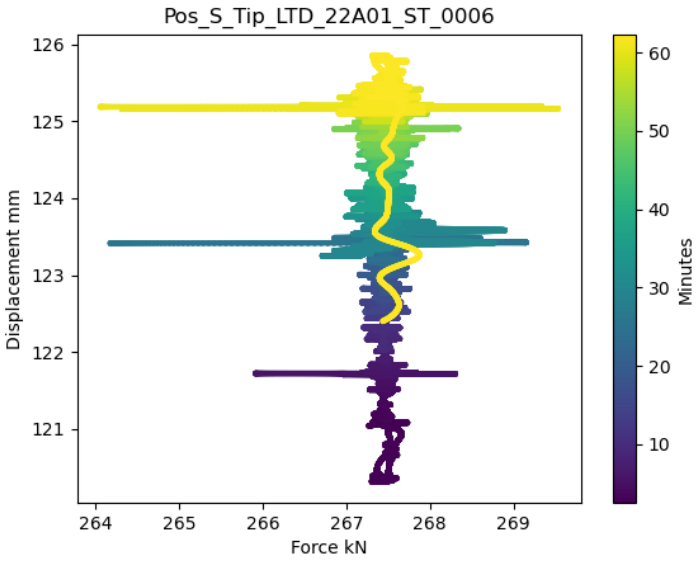

Figure 6.10: Displacement vs force vs time during first static test

Figure 6.10 shows how the displacement of the tip of the blade varies with force and time. It can be seen that an average force of approximately 267.5 kN was applied throughout the test, with occasional spikes (a result of the motion of the saddle which was corrected in subsequent tests). As the test progresses the displacement of the tip of the blade increased from 120.5 mm to almost 126 mm. This increase in displacement over time would normally indicate a decrease in stiffness from damage to the blade. However, due to the slipping of the saddle during the test, altering the loading conditions, it is not possible to say definitively that the increase in displacement was from damage. From looking at the natural frequency test data, it is clear that the frequency reduced as a result of the static test, confirming that damage started occuring during the static test.

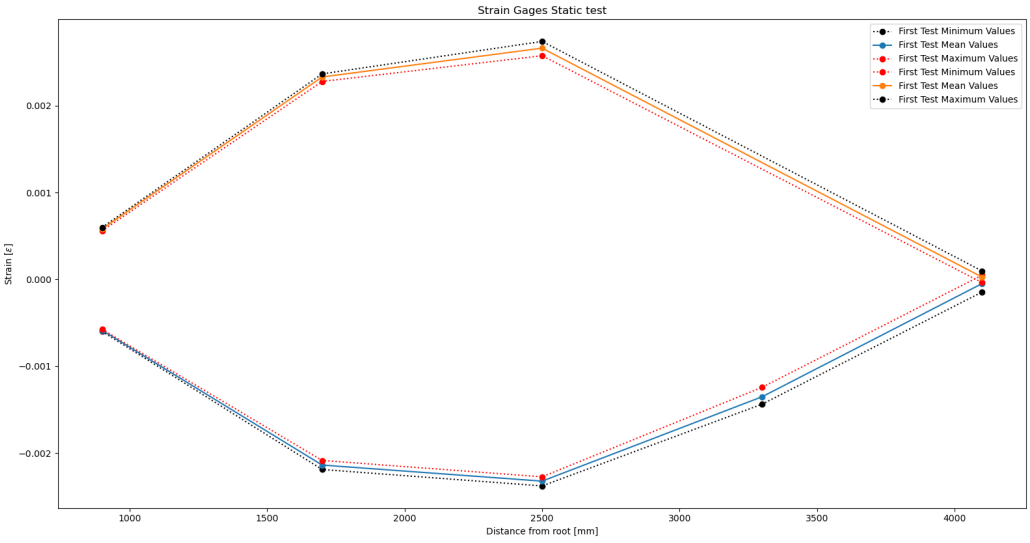

Figure 6.11: Strain along the blade - initial static test

Figure 6.11 shows the strain variation along the length of the blade, the values shown here are the average strains measured during the static test 1 hour hold. The strain gauges used to generate this data were those shown in table 6.4, along the centre of the top and bottom of the blade. It can be seen that the peak strain observed was at 2500mm from the root of the blade. Closer to the root, the stiffness of the composite in combination with the steel root connection means that very little deformation is observed. The strain gauge at 3300mm on the bottom of the blade, was positioned close to the loading saddle and was damaged when the saddle slipped during the test, resulting in the missing data. As expected the strain gauges beyond the loading saddle at 4100mm read close to 0, as this area of the blade moves with the actuator rather than being constrained and deforming.

Strain Gauge Selection	
Gauges on Top Surface	Gauges on Bottom Surface
Str-Ros-120-1-1-0	Str-Ros-120-1-4-0
Str-Ros-120-2-1-0	Str-Ros-120-2-4-0
Str-Ros-120-3-1-0	Str-Ros-120-3-4-0
Str-Ros-120-4-1-0	Str-Ros-120-4-4-0 (Failed)
Str-Ros-120-5-1-0	Str-Ros-120-5-4-0

Table 6.4: Selected gauges for static strain analysis

6.4.2 Final Static Test Run

After the fatigue testing was completed a further static test was carried out with the same load profile as the initial static test. The force-time graph for this test can be seen in Figure 6.12. The test used the same target load and duration. When comparing Figure 6.9 to Figure 6.12 it can be seen that the final static test load signal is significantly noisier. This is a result of the change in load saddle from the soft rubber of the articulated saddle to the relatively stiff MDF saddle.

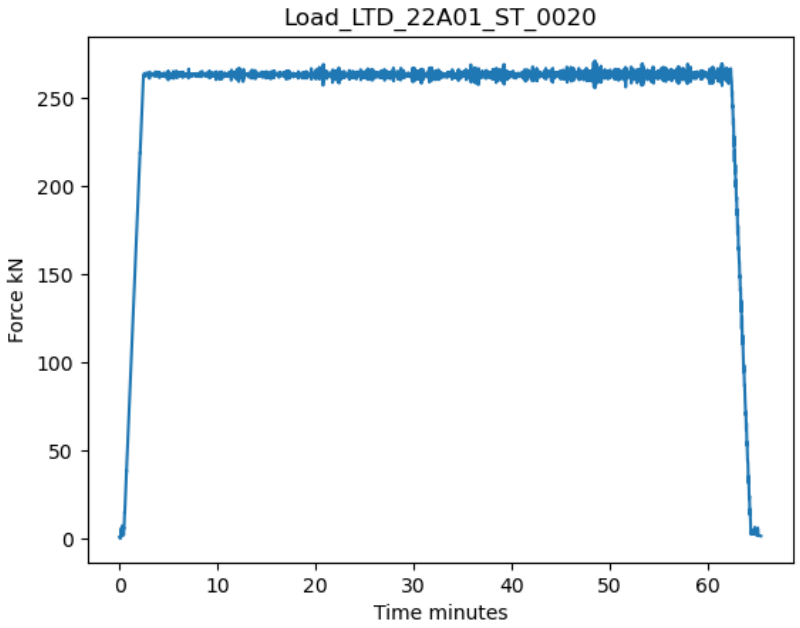

Figure 6.12: Full final static loading cycle

Figure 6.13 shows how the displacement of the tip of the blade varies with force and time. When

compared to the first static test, increased variation in force can be seen. This is likely due to the increased stiffness of the loading saddle responding to the digital hydraulic system. The slightly lower displacement is likely due to the slightly reduced force observed during the test. There is also a less extreme change of position with time, on average only seeing approximately 2mm of displacement variation from the start to the end of the test compared to a 5mm variation from the first static test.

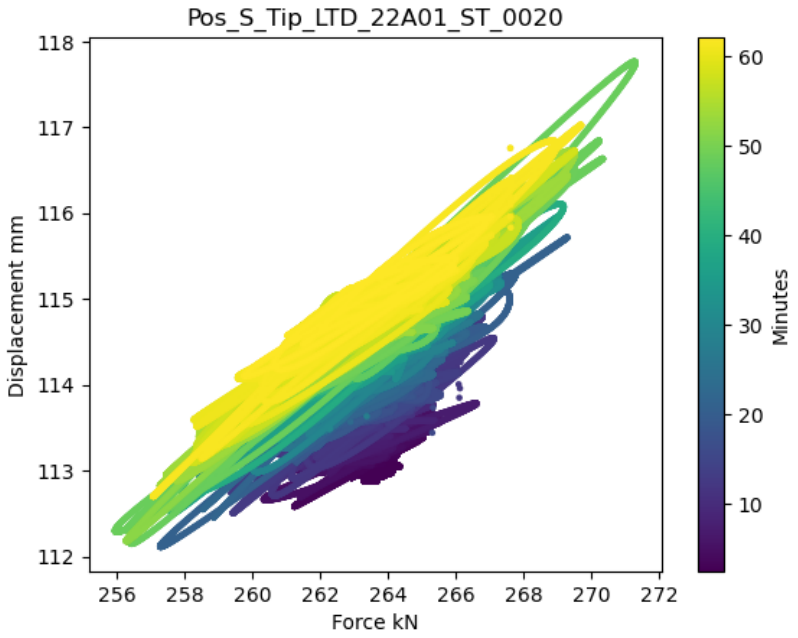

Figure 6.13: Displacement vs force vs time during final static test

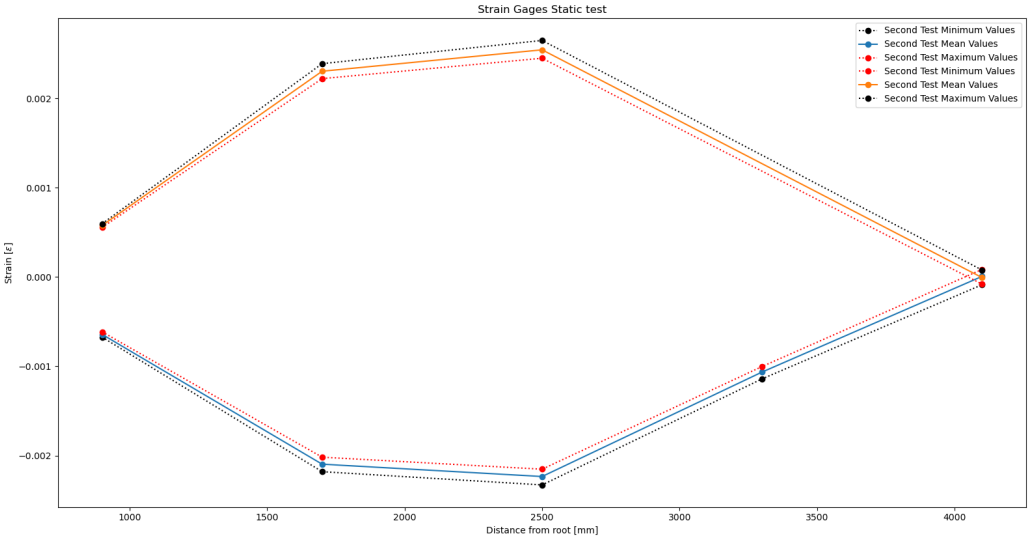

Figure 6.14: Strain along the blade - final static test

Figure 6.14 shows the strain variation along the length of the blade during the final static test the

values shown here are equivalent to those from the initial test shown in Figure 6.11.

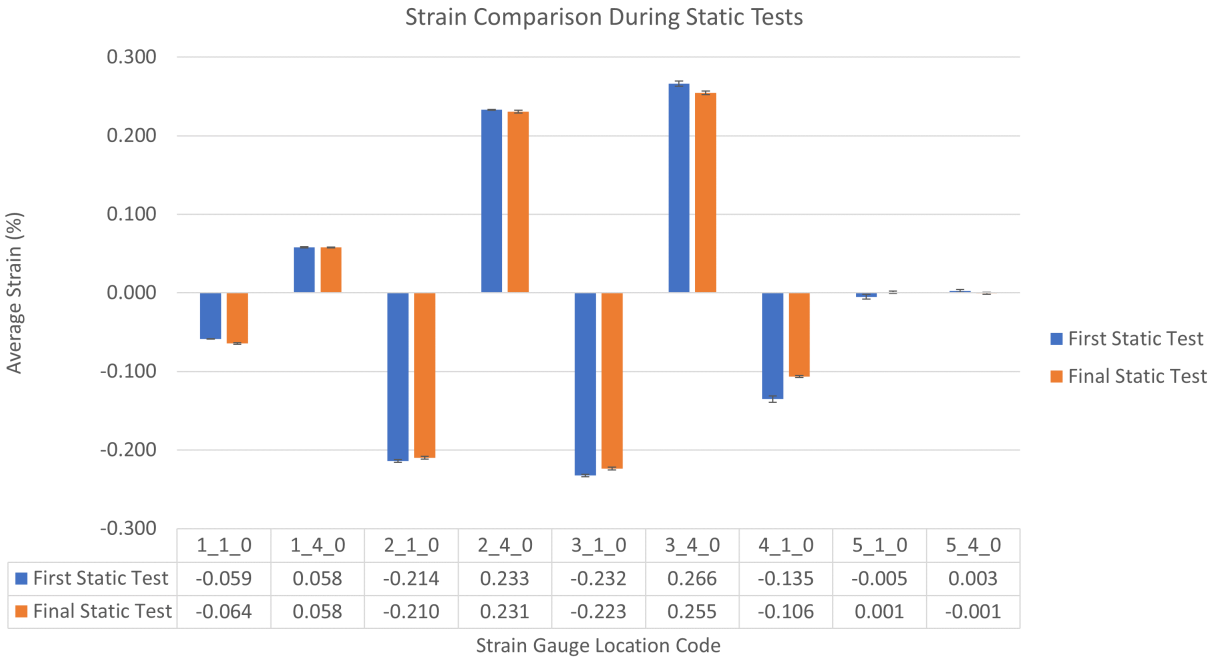

	1_1_0	1_4_0	2_1_0	2_4_0	3_1_0	3_4_0	4_1_0	5_1_0	5_4_0
First Static Test	-0.059	0.058	-0.214	0.233	-0.232	0.266	-0.135	-0.005	0.003
Final Static Test	-0.064	0.058	-0.210	0.231	-0.223	0.255	-0.106	0.001	-0.001

Figure 6.15: Strain Comparison During Static Tests

A comparison between the average strain in the initial static and in the final static test can be seen in Figure 6.15 where it can be seen that in almost all cases the strain values reduced slightly. This is likely an effect of the change of the loading saddle which slightly altered the load location and angle of load introduction from the first to the second test. It is likely that damage has occurred between the tests but the change in saddle makes it difficult to be certain of the source of the observed variations.

6.4.3 DIC Static Results

During the initial static test, DIC was used to map the strain over the entire speckled surface of the blade.

The following settings (figure 6.5) were used for the DIC correlation using the MatchID 3D DIC software.

DIC settings	
Subset size	21
Step size	10
Criterion	ZNSSD
Interpolation	Local Bicubic Splin
Shape function	Affine
Stereo Transformation	Affine
Prefiltering	Gaussian
Progress history	Spatial
Strain Settings	
Strain Window	15
Virtual Strain Gauge	161
Strain Interpolation	Q9
Strain Tensor	Euler-Almansi

Table 6.5: DIC Settings Used

Seen in figure 6.16 is the strain map during the first static test. It is important to note, that in the edges of the areas used for strain mapping, the difficulty in correlating the change in distances between speckles led to large overshoots of strain measurements

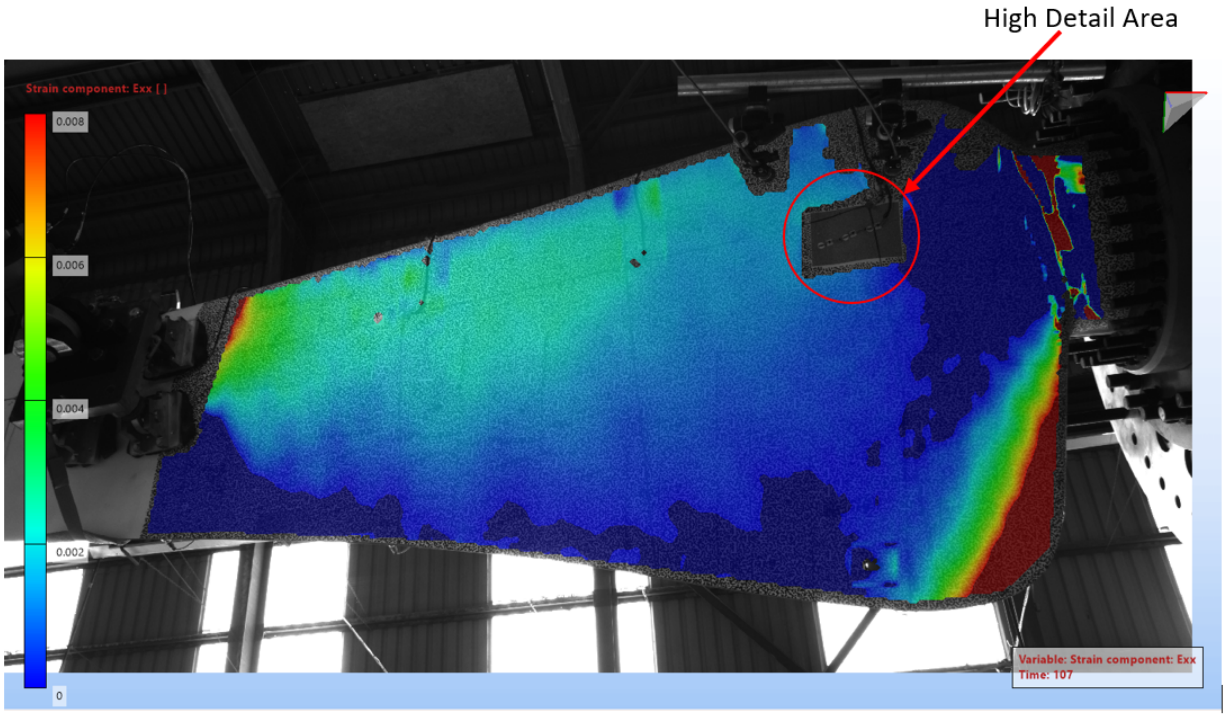

Figure 6.16: DIC Engineering Strain Overview

To ensure the data obtained was reliable, the longitudinal strains were extracted using the MatchID 3D DIC software. By analysing the strain in an area close to location of the strain gauge at 2_4_0 and 3_4_0 the strains from the DIC can be compared with the actual strain measured by the strain gauges. Results for this are seen in figure 6.17. The strain profiles at each of these locations are seen in figures 6.18 and 6.19. The average strain at point 2_4_0 for the holding period of the test was found to be 0.00228 and at point 3_4_0 the average strain was found to be 0.00244.

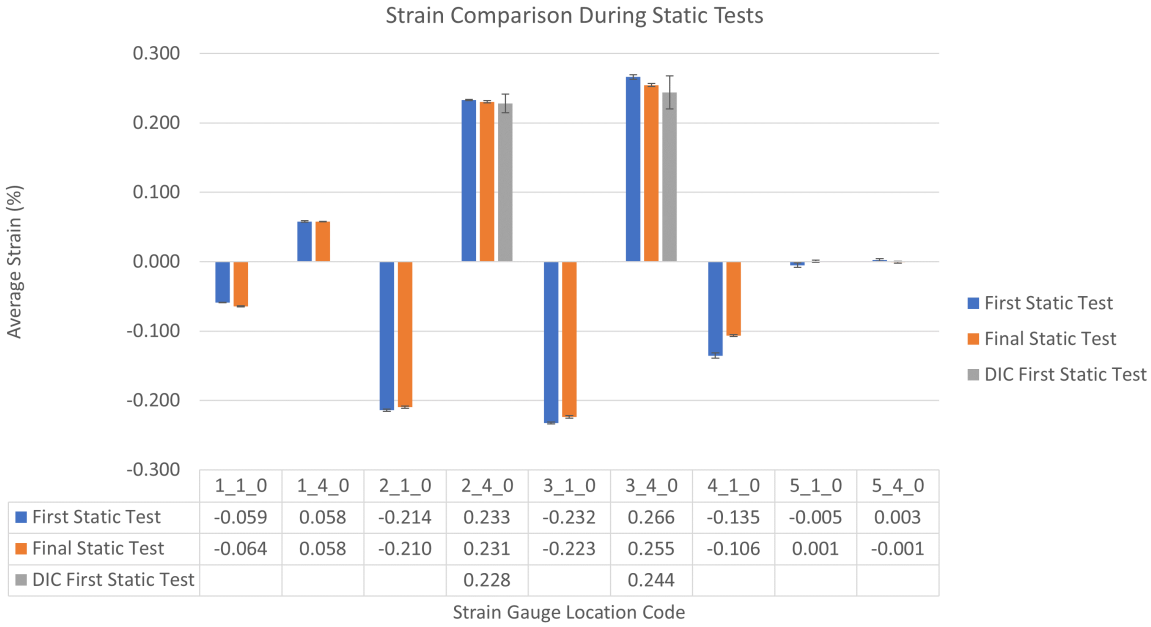

	1_1_0	1_4_0	2_1_0	2_4_0	3_1_0	3_4_0	4_1_0	5_1_0	5_4_0
First Static Test	-0.059	0.058	-0.214	0.233	-0.232	0.266	-0.135	-0.005	0.003
Final Static Test	-0.064	0.058	-0.210	0.231	-0.223	0.255	-0.106	0.001	-0.001
DIC First Static Test				0.228		0.244			

Figure 6.17: Strain Comparison During Static Tests with DIC Results

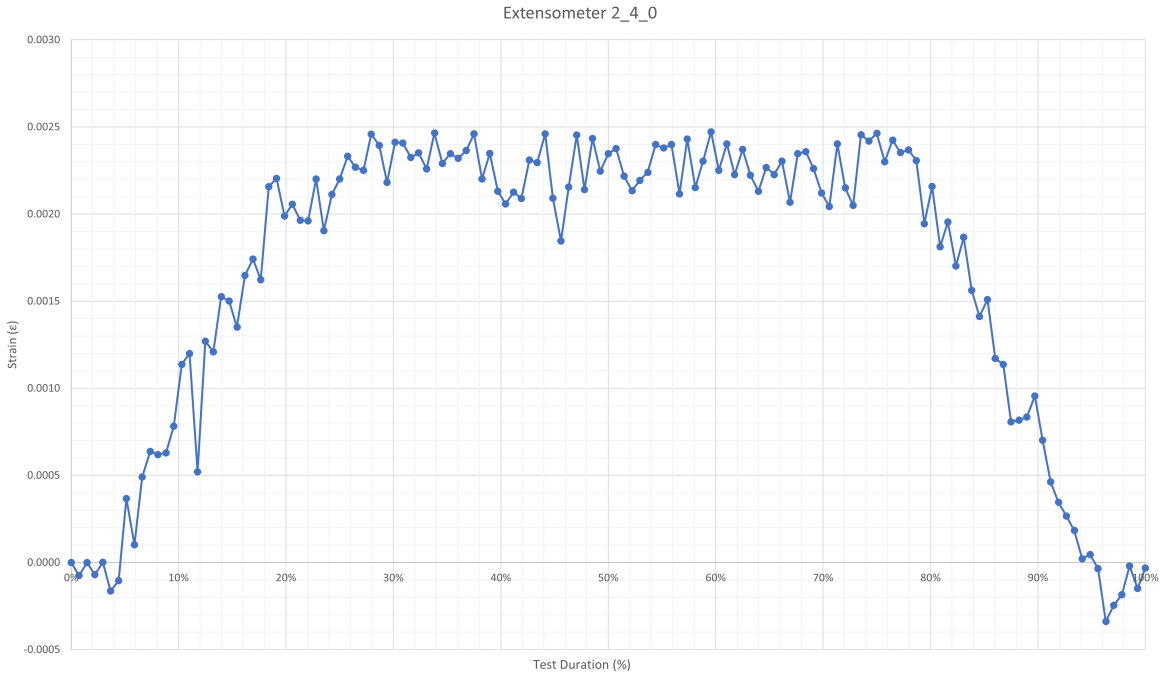

Figure 6.18: Strain at location 2_4_0

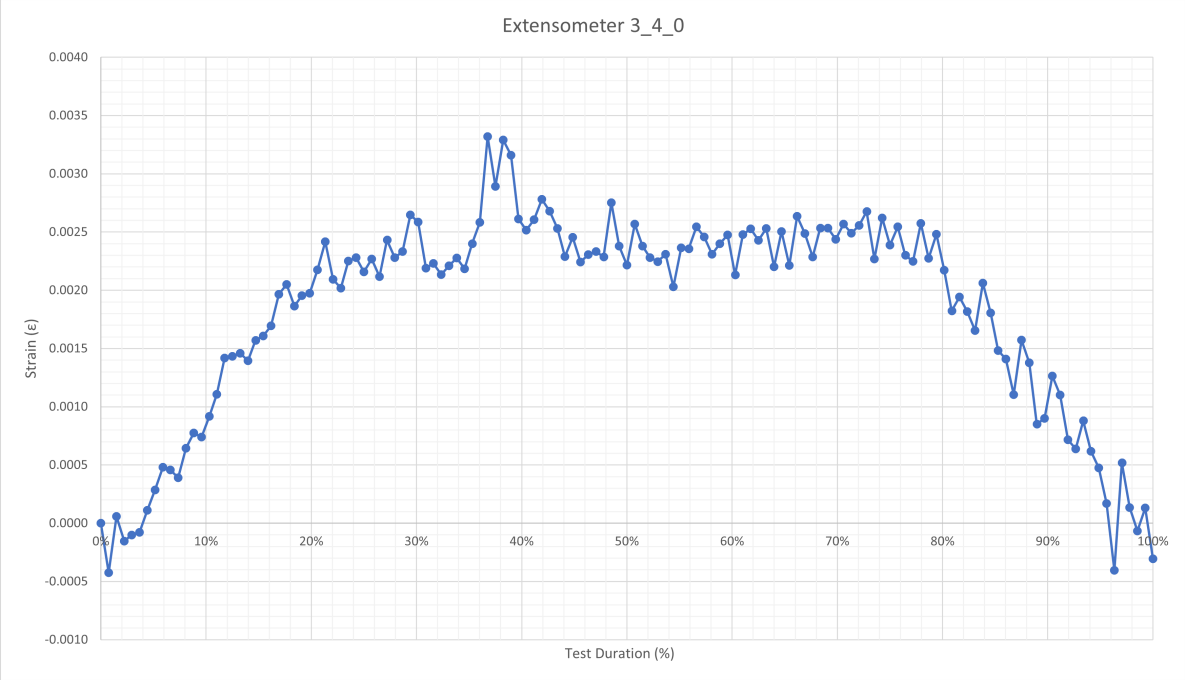

Figure 6.19: Strain at location 3_4_0

These figures show that the DIC strain captures the same trends in strain as the rosette gauges, showing the same increases and drops along and strain values very similar to those measured by the gauges. Therefore, the DIC system can be reliably used for both in-depth analysis locally to strain gauges where the data can be validated. Also, to identify regions of high strain values or gradients within the blade. From the investigation carried out, no areas of excessively high strain (which were not attributable to edge effects of the correlation algorithm) were detected.

To visualise the strain along the blade, a line was analysed as seen in figure 6.20

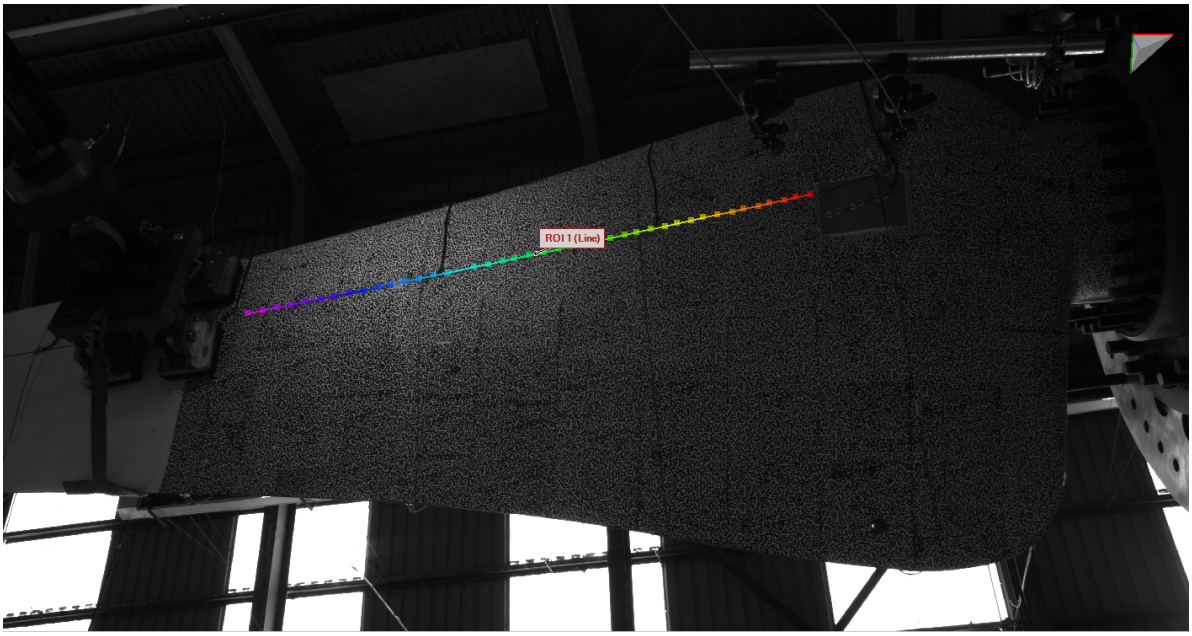

Figure 6.20: Line used for extraction of strain

The strain along the blade is seen in figure 6.21. This highlights that the edges of the regions of strain mapping have very high strain values due to the difficulty in correlating these areas. As seen in the first few data points on the graph.

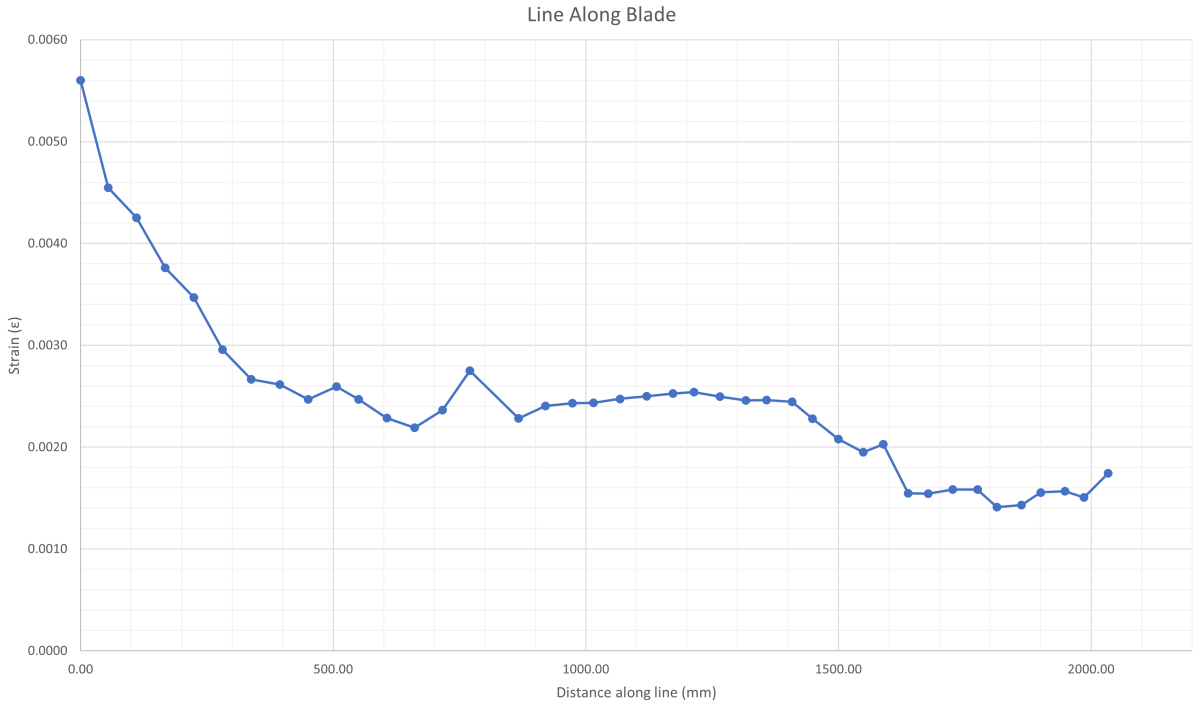

Figure 6.21: Strain along the blade

6.5 Fatigue Test Results

Throughout the fatigue test 31,775 cycles were completed. This is equivalent to approximately 21.7 years of tidal cycles.

6.5.1 Load

Results for the applied load delta to the blade are seen in figure 6.22. The average Δ Force was 155.46 kN and the target Δ Force was 165.34 kN. It is noted that throughout the test the delta load decreases. The average load ratio (R number) for the test was 0.14, the target was 0.1. The large spike in load occurs every time the fatigue testing is restarted and included here for completeness. The large ramp-up in load over the first 3000 cycles was a result of incorrect gains being set during the PID tuning of the test. This was improved as the test continued and is provided here again for complete transparency of the test data.

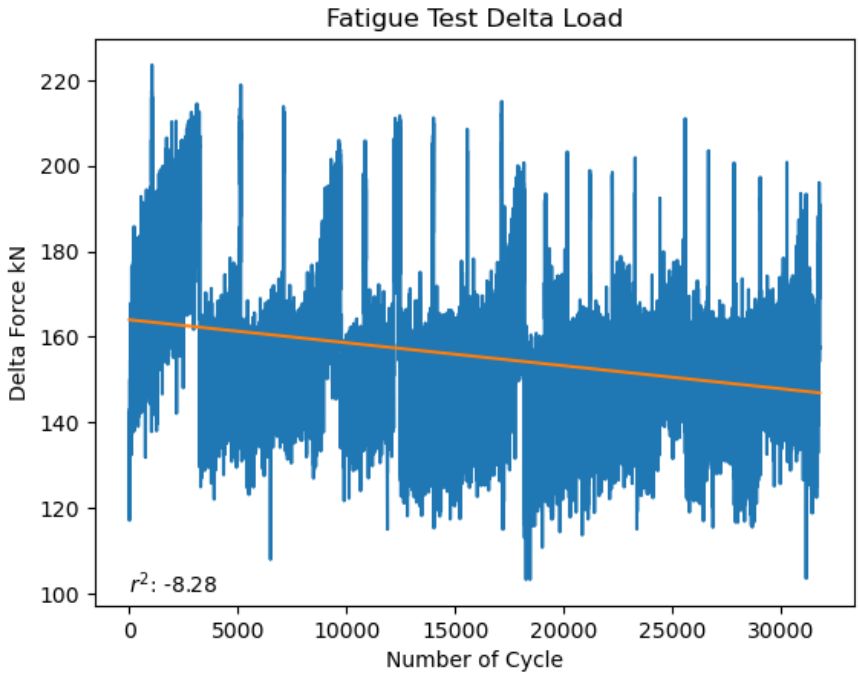

Figure 6.22: Load Delta

Figure 6.23 shows how the relationship between tip displacement and force varies throughout the test. The trend line shows a slight downward trend which would indicate an increase in blade stiffness but it is too subtle a change to draw any definitive conclusions. The fall in stiffness between 20,000 and 25,000 cycles would also require additional testing and analysis beyond the scope of this report to draw any conclusions.

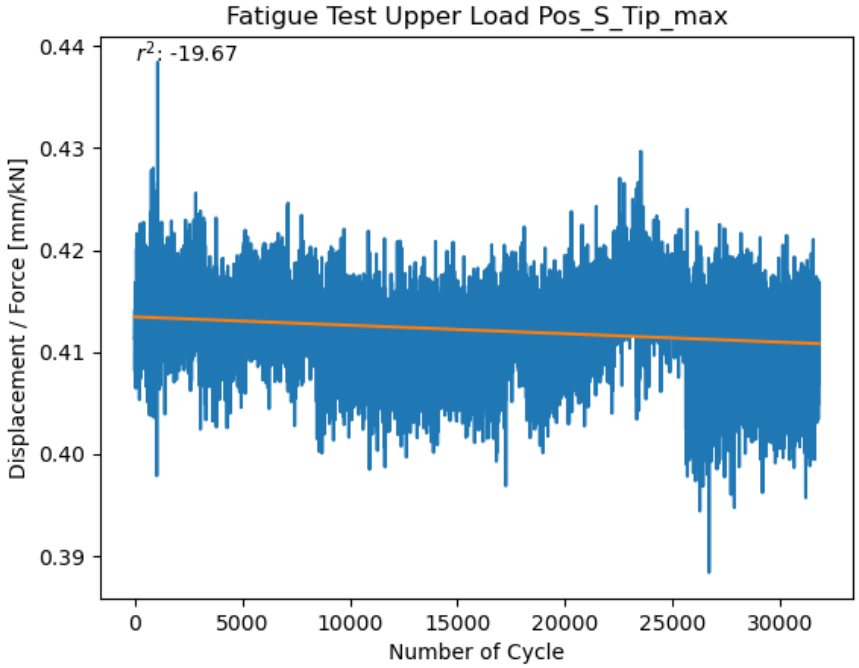

Figure 6.23: Blade tip Displacement/Force variations

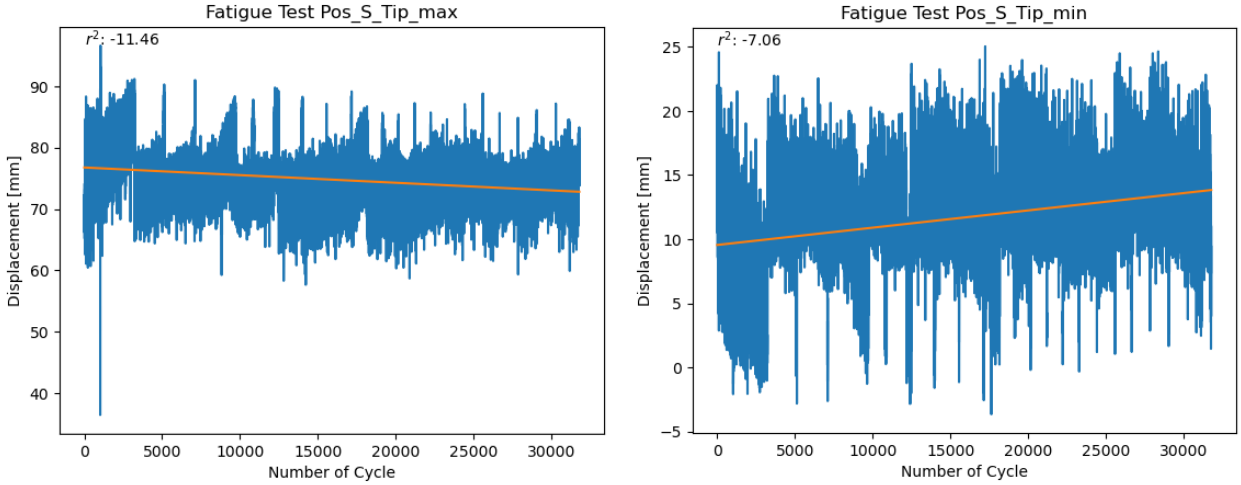

(a) Max **(b)** Min

Figure 6.24: Tip displacement during the fatigue test

It is seen in figure 6.24 that throughout the test the blade does not return to the same position. The maximum displacement reduces over time and the minimum increases, combining to result in a reduced Δ displacement.

6.5.2 Strain

Figure 6.25b indicates that throughout the test, at equivalent loads, the strain in the blade decreased (ie more compression). This suggests that the blade at this location (1_1_0) has reduced in stiffness. Figure 6.25a also indicates this with the downward trending line. Similar behaviour is seen at locations 3_1_0 and 3_4_0 (figures 6.26 and 6.27)

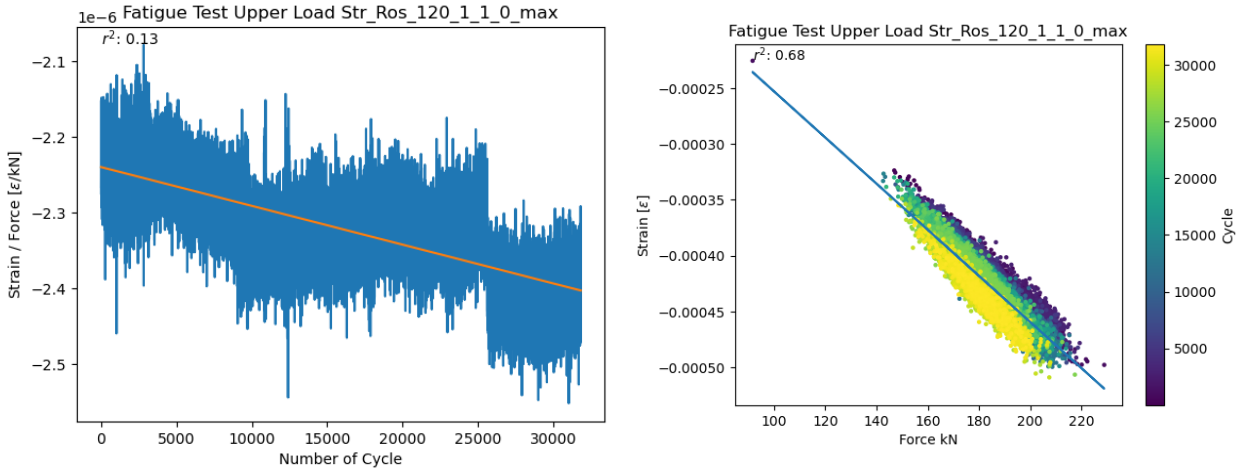

(a) Strain/Force

(b) Strain vs Load

Figure 6.25: Blade top surface strain 900mm from root

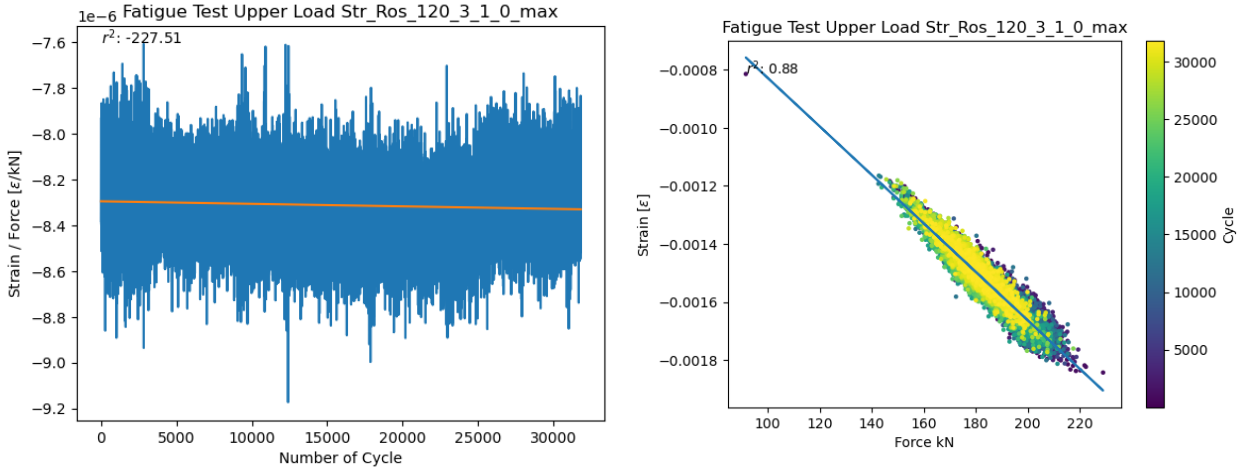

(a) Strain/Force

(b) Strain vs Load

Figure 6.26: Blade top surface strain 2500mm from root

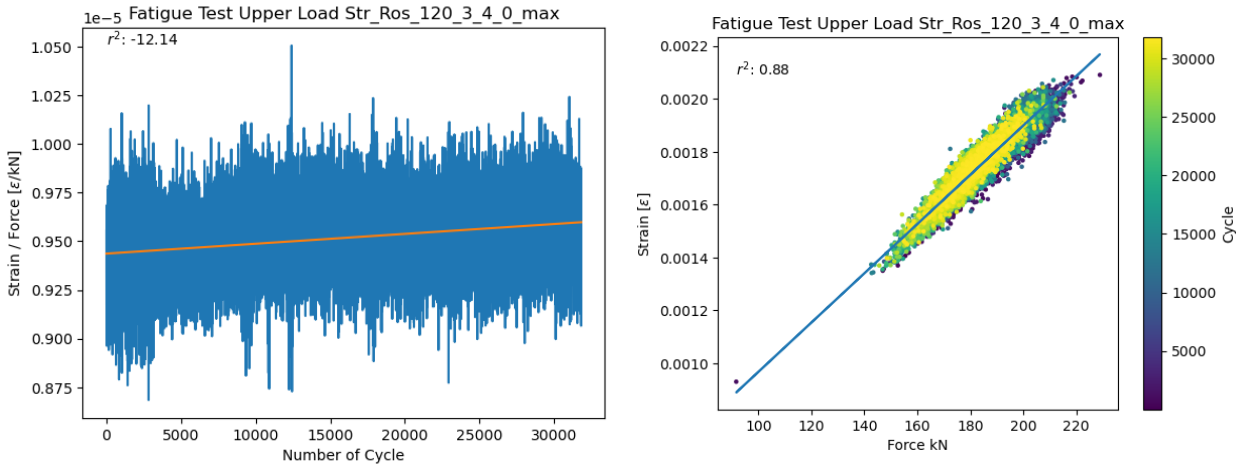

(a) Strain/Force

(b) Strain vs Load

Figure 6.27: Blade bottom surface strain 2500mm from root

7 Deviation and Unexpected Behaviour

During the initial static test the saddle experienced some movement. This resulted in the load not being applied to the same location throughout the test. This was corrected in subsequent tests by using a different type of loading saddle that clamped to the blade rather than resting against it. This change resulted in a different loading system stiffness and a slight alteration to the load distribution into the blade.

PID tuning of the control system was extremely delicate and the auto-tuning system was not able to adequately achieve the desired performance. This meant that the tuning had to be carried out at the actual fatigue loads under the real test conditions. This resulted in load cycles being applied to the blade which either overshot or undershot targets during tuning.

The control system exhibited occasional lag spikes, resulting in the control loop stopping and requiring a restart. The resultant overshoots can be seen in the test data.

Signal noise was higher than expected on several of the connected sensors. This resulted in some juddering around the top and bottom of the loading cycles during fatigue and during the holding period of the static testing. A lot of the noise was addressed with low pass filters but this wasn't always possible. The noise was due to the length of the signal cables connected to the sensors and the stability of the DC power supplies.

One of the strain gauges connected to the bottom side of the blade failed as a result of the saddle slipping during the first static test and repair was not possible.

The temperature of the test hall varied by up to 10°C throughout testing. Where possible this was addressed through the calibration procedures for the strain gauges and other sensors but the temperature variation during extended test periods could not be accounted for.

8 Evaluation of Tests

As this was a research test, not a certification test there was no design requirements to certify against.

8.1 Evaluation of Test Loads

As no specific load cases were defined or modelled for the testing. The loading was estimated from simulations from Oxford University and the original blade design. However, no expected strain, or deflections were available to compare against

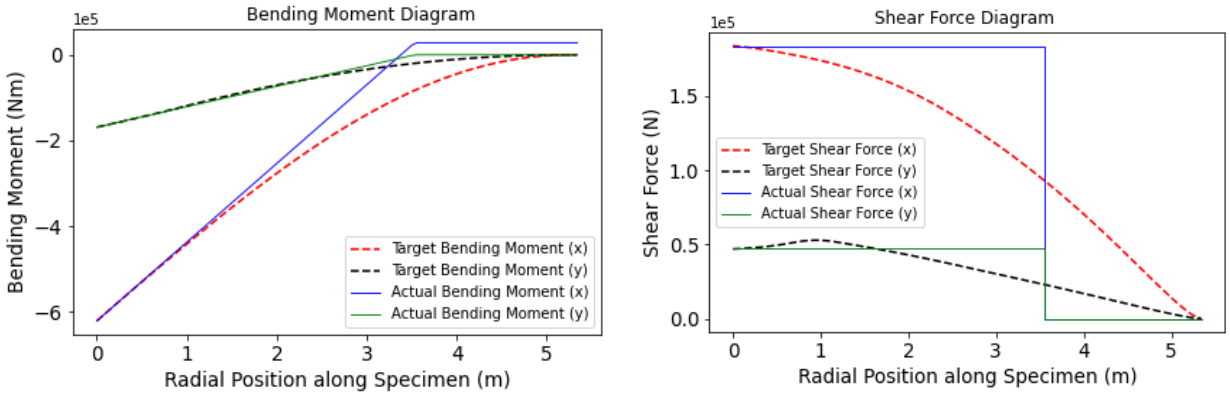

(a) BMD **(b)** SFD

Figure 8.1: Bending moment and shear force diagrams using predicted values from Oxford data

8.2 Evaluation of Blade Stiffness

The blade stiffness was evaluated at both the tip and the centre of the blade where the displacement measurements were made. The results of this evaluation can be seen in Figure 8.2 and Table 8.1.

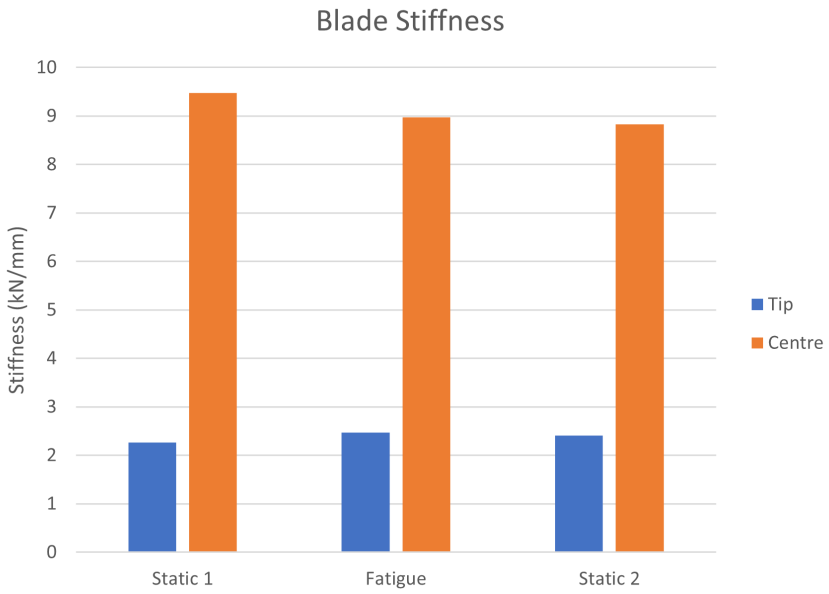

Figure 8.2: Blade stiffness at centre and tip

Test	Location	Displacement (mm)	Load (kN)	Stiffness (kN/mm)
Static 1	Tip	120.2	272.83	2.26
	Centre	28.8	272.83	9.47
Fatigue	Tip	68.67	169.64	2.47
	Centre	18.91	169.64	8.97
Static 2	Tip	114.53	275.99	2.41
	Centre	31.24	275.99	8.83

Table 8.1: Blade Stiffness

9 Conclusions

- The blade survived the worst-case static load criteria as defined by the blade developer.
- The blade withstood 20 years (equivalent) of accelerated fatigue loading without catastrophic failure.
- The natural frequency decreased during the testing, from 18.03 Hz to 17.93 Hz. It is likely that this is a result of minor damage to areas of the blade, but the change may be influenced by other factors such as root connection bolt tension variations.
- As the blade met the requirements set out in the load conditions from the blade developer, it appears that the time the blade spent deployed in the ocean has not negatively affected its ability to withstand an additional 20 years of loading.
- No specific failures were observed throughout all testing. No audible sounds of failure were detected, and no sudden changes in position or load. The DIC system did not detect any areas of exceptionally raised strain. The highest strain measured with strain gauges was 0.266 % on the bottom surface of the blade, near the loading saddle.
- Multiple improvements to the testing procedure have been identified during this test including control strategies, load introduction, instrumentation layout, instrument calibration, and test design.
- To detect a catastrophic failure, the blade would have to be pushed significantly beyond the extreme loading cases designed for by the developer or modelled by Oxford University. This falls outside the scope of this project.

References

[1] *Ripples of anxiety.* [Online]. Available: https://www.imeche.org/news/news-article/ripples-of-anxiety.

[2] C. Huxley-Reynard, J. Thake, and G. Gibberd, "TG-RE-040-0091 Rev B Deepgen Blade Design Report," TIDAL GENERATION LTD SETsquared Business Acceleration Centre, Bristol, Tech. Rep., Mar. 2008.

[3] British Standards Institution, *Marine energy. Wave, tidal and other water current converters. Part 3, Measurement of mechanical loads.* P. 96, ISBN: 9780580994944.

[4] C. Huxley-Reynard, J. King, and G. Gibberd, "TG-RE-000-0081 Rev D Extreme and Fatigue Load Calculations for Deepgen 500kW Tidal Turbine," TIDAL GENERATION LTD SETsquared Business Acceleration Centre, Bristol, Tech. Rep., May 2008.

[5] P. Williams and C. O Bradaigh, *Investigation of load introduction methods from hydraulic test actuators to composite test specimens in the FASTBLADE facility*, 2021.

[6] M. Angel Valdivia Camacho and C. Ó Brádaigh, *Parasitic Effects of Load Introduction Points on Tidal Turbine Blades in Full Scale Static and Fatigue Testing Procedures*, 2020.

[7] Brian Sellar, *Met-Ocean Data Science for Offshore Renewable Energy Applications*, May 2017. [Online]. Available: https://redapt.eng.ed.ac.uk/#.

[8] B. G. Sellar, G. Wakelam, D. R. J. Sutherland, D. M. Ingram, and V. Venugopal, "Characterisation of Tidal Flows at the European Marine Energy Centre in the Absence of Ocean Waves," *Energies*, vol. 11, no. 1, 2018, ISSN: 1996-1073. DOI: 10.3390/en11010176. [Online]. Available: https://www.mdpi.com/1996-1073/11/1/176.

Appendix A Blade Description According to IEC/TC 62600-3 Annex A.6.2

A.6.2 Blade description

The blade description in the test plan should be sufficient to ensure that the blade will fit the test stand and avoid unintended overloading during storage, handling, lifting, mounting and testing in the laboratory.

The following information should be supplied:

- blade geometry (preferably in form of a drawing):
  - blade length;
  - chord and twist distribution;
  - pre-bend or sweep;
- mass and centre of gravity;
- blade surface condition;
- blade mounting details:
  - bolt pattern (including tolerances) and interface dimension;
  - bolt size, type and grade;
  - bolt clamping length;
  - bolt pretension or torque procedure;
- lifting and handling procedures;
- maximum expected deflections under load;
- profile geometry at load introduction points.

Additional information (such as the stiffness of the mounting structure) may be required depending on the test specifics.

Figure A.1: Blade Description as required by the IEC TS -62600-3:2020 Test Standard [3]

BLADE OUTER GEOMETRY						SPAR CAPS (80% UD Carbon)						SPAR SHEAR WEBS (+/-45deg Carbon)		RIBS (+/- 45deg glass)	
Element ID	Distance from hub CtLine)	Chord	Twist	Blade overall thickness	t/c ratio	Spar height	No. Top Plies	No. Btm Plies	Width (material laid flat)	Top cap thickness (with 10% de plies)	Btm cap thickness (with 10% de plies)	Shear web height (material laid flat)	Spar wall thickness	Rib position	Rib thickness (2 off)
[-]	[mm]	[mm]	[deg]	[mm]	[-]	[mm]	[-]	[-]	[mm]	[mm]	[mm]	[mm]	[mm]	[-]	[mm]
0	1000.0	660.3	31.9			517.6	-	-	517.6						
1	1100.0	953.3	30.1			511.9	18	11	511.9	12.9	8.0	491.0			
2	1200.0	1187.9	28.5		0.3	506.1	22	14	506.1	16.3	10.2	479.7	8.4		
3	1300.0	1372.1	27.0		0.3	500.3	27	17	500.3	19.7	12.3	468.3	8.4		
4	1400.0	1512.9	25.6		0.3	494.6	32	20	494.6	22.1	14.5	457.0	9.0		
5	1500.0	1616.7	24.3		0.3	488.8	37	23	488.8	26.5	16.7	445.6	9.0		
6	1600.0	1689.3	23.0		0.3	483.0	41	26	483.0	29.9	18.9	434.3	9.0	X	3.0
7	1700.0	1735.8	21.9		0.3	477.3	46	29	477.3	33.3	21.1	422.9	9.0		
8	1800.0	1760.7	20.9		0.2	471.5	51	32	471.5	36.7	23.2	411.6	9.0		
9	1900.0	1768.1	19.9		0.2	465.8	56	35	465.8	40.1	25.4	400.2	9.0		
10	2000.0	1761.3	19.0	480.0	0.2	460.0	60	38	460.0	43.6	27.6	388.9	9.0	X	3.0
11	2100.0	1743.5	18.1	463.0	0.2	443.0	56	35	454.5	40.1	25.4	377.4	9.0		
12	2200.0	1717.1	17.3	446.0	0.2	426.0	51	32	449.0	36.7	23.2	366.0	8.4		
13	2300.0	1684.6	16.6	429.0	0.2	409.0	46	29	443.5	33.3	21.1	354.6	8.4		
14	2400.0	1647.7	15.9	412.0	0.2	392.0	41	26	438.1	29.9	18.9	343.2	7.8	X	3.0
15	2500.0	1608.0	15.3	395.0	0.2	375.0	37	23	432.6	26.5	16.7	331.8	7.8		
16	2600.0	1566.7	14.7	378.0	0.2	358.0	32	20	427.1	23.1	14.5	320.4	7.8		
17	2700.0	1525.0	14.1	361.0	0.2	341.0	27	17	421.6	19.7	12.3	309.0	7.2		
18	2800.0	1483.6	13.6	344.0	0.2	324.0	22	14	416.1	16.3	10.2	297.6	7.2	X	3.0
19	2900.0	1443.1	13.1	327.0	0.2	307.0	18	11	410.6	12.9	8.0	286.2	6.6		
20	3000.0	1404.0	12.6	310.0	0.2	290.0	13	9	405.1	9.4	6.5	274.0	6.6		
21	3100.0	1366.5	12.1	298.4	0.2	278.4	13	9	399.6	9.4	6.5	262.4	6.6		
22	3200.0	1330.9	11.7	286.7	0.2	266.7	13	9	394.2	9.4	6.5	249.8	7.2	X	3.0
23	3300.0	1297.1	11.3	273.8	0.2	253.8	13	9	388.7	9.4	6.5	237.8	7.2		
24	3400.0	1266.3	10.9	262.4	0.2	242.4	13	9	383.2	9.4	6.5	226.5	7.2		
25	3500.0	1238.3	10.6	251.8	0.2	231.8	13	9	377.7	9.4	6.5	215.8	7.2		
26	3600.0	1209.0	10.2	241.7	0.2	221.7	13	9	372.2	9.4	6.5	205.7	7.2	X	3.0
27	3700.0	1180.2	9.9	232.2	0.2	212.2	13	9	366.7	9.4	6.5	196.2	7.2		
28	3800.0	1154.8	9.6	223.3	0.2	203.3	12	9	361.2	8.7	6.5	188.0	7.2		
29	3900.0	1130.5	9.3	214.9	0.2	194.9	12	9	355.8	8.7	6.5	179.7	7.2		
30	4000.0	1107.3	9.0	207.0	0.2	187.0	12	8	350.3	8.7	5.8	172.5	7.2	X	3.0
31	4100.0	1085.0	8.7	199.7	0.2	179.7	11	8	344.8	8.0	5.8	165.9	7.2		
32	4200.0	1063.3	8.4	192.9	0.2	172.9	11	8	339.3	8.0	5.8	159.0	7.2		
33	4300.0	1042.2	8.2	186.4	0.2	166.4	10	8	333.8	7.3	5.8	153.3	7.2		
34	4400.0	1021.6	7.9	180.4	0.2	160.4	10	7	328.3	7.3	5.1	148.1	7.2	X	3.0
35	4500.0	1001.4	7.7	174.8	0.2	154.8	9	7	322.8	6.5	5.1	143.2	7.2		
36	4600.0	981.6	7.5	169.6	0.2	149.6	9	6	317.3	6.5	4.4	138.8	7.2		
37	4700.0	962.2	7.3	164.8	0.2	144.8	8	6	311.9	5.8	4.4	134.7	6.6		
38	4800.0	943.3	7.1	160.4	0.2	140.4	7	6	306.4	5.1	4.4	130.9	6.6	X	3.0
39	4900.0	924.7	6.9	156.2	0.2	136.2	6	4	300.9	4.4	2.9	129.0	6.0		
40	5000.0	906.8	6.7	152.4	0.2	132.4	6	4	295.4	4.4	2.9	125.1	5.4		
41	5100.0	889.4	6.5	148.8	0.2	128.8	5	4	289.9	3.6	2.9	122.3	5.4		
42	5200.0	872.8	6.3	145.5	0.2	125.5	4	3	284.4	2.9	2.2	120.4	4.8	X	3.0
43	5300.0	857.0	6.2	142.4	0.2	122.4	3	3	278.9	2.2	2.2	118.1	4.8		
44	5400.0	842.1	6.0	139.6	0.2	119.6	3	3	273.4	2.2	2.2	115.2	4.2		
45	5500.0	828.1	5.8	136.9	0.2	116.9	3	3	268.0	2.2	2.2	112.5	3.6		
46	5600.0	814.9	5.7	134.4	0.2	114.4	3	3	262.5	2.2	2.2	110.0	3.6	X	3.0
47	5700.0	802.6	5.6	132.0	0.2	112.0	3	3	257.0	2.2	2.2	107.7	3.0		
48	5800.0	791.0	5.4	129.8	0.2	109.8	3	3	251.5	2.2	2.2	105.4	3.0		
49	5900.0	779.8	5.3	127.7	0.2	107.7	3	3	246.0	2.2	2.2	103.3	3.0		
50	6000.0	768.7	5.2	125.6	0.2	105.6	3	3	240.5	2.2	2.2	101.3	3.0	X	3.0
51	6100.0	757.1	5.0	123.6	0.2	103.6	3	3	235.0	2.2	2.2	99.3	3.0		
52	6200.0	744.4	4.9	121.5	0.2	101.5	3	3	229.6	2.2	2.2	97.1	3.0		
53	6250.0	739.0	4.8	120.6	0.2	100.6	3	3	226.8	2.2	2.2	96.2	3.0	X	3.0

Figure A.2: Detailed Description of the Blade Geometry along the Blade Span [2]